Isotopic signatures of production and uptake of H_2 by soil

Qianjie Chen[1, 2], Maria E Popa[1], Anneke M Batenburg[1, 3], and Thomas Röckmann[1]

[1] Institute for Marine and Atmospheric research Utrecht, Utrecht University, The Netherlands

[2] Department of Atmospheric Sciences, University of Washington, Seattle, Washington, USA

[3] Department of Applied Physics, University of Eastern Finland, Kuopio, Finland

Abstract: Molecular hydrogen (H_2) is the second most abundant reduced trace gas (after methane) in the atmosphere, but its biogeochemical cycle is not well understood. Our study focuses on the soil production and uptake of H_2 and the associated isotope effects. Air samples from a grass field and a forest site in the Netherlands were collected using soil chambers. The results show that uptake and emission of H_2 occurred simultaneously at all sampling sites, with strongest emission at the grassland sites where clover (N_2 fixing legume) was present. The H_2 mole fraction and deuterium content were measured in the laboratory to determine the isotopic fractionation factor during H_2 soil uptake (α_{soil}) and the isotopic signature of H_2 that is simultaneously emitted from the soil (δD_{soil}). By considering all net-uptake experiments, an overall fractionation factor for deposition of $\alpha_{soil} = k_{HD} / k_{HH} = 0.945 \pm 0.004$ (95% CI) was obtained. The difference in mean α_{soil} between the forest soil 0.937 ± 0.008 and the grassland 0.951 ± 0.025 is not statistically significant. For two experiments, the removal of soil cover increased the deposition velocity (v_d) and α_{soil} simultaneously, but a general positive correlation between v_d and α_{soil} was not found in this study. When the data are evaluated with a model of simultaneous production and uptake, the isotopic composition of H_2 that is emitted at the grassland site is calculated as $\delta D_{soil} = (-530 \pm 40)$ ‰. This is less deuterium-depleted than what is expected from isotope equilibrium between H_2O and H_2.

1. Introduction

H_2 is considered as alternative energy carrier to replace fossil fuels in the future. However, the environmental and climate impact of a potential widespread use of H_2 is still under assessment. Several studies suggested that the atmospheric H_2 mole fraction might increase substantially in the future due to the leakage during production, storage, transportation and use of H_2, which could significantly affect atmospheric chemistry (Schultz et al., 2003; Tromp et al., 2003; van Ruijven et al., 2011; Warwick et al., 2004).

In the troposphere, H_2 has a mole fraction of about 550 parts per billion (ppb = nmol mol^{-1}) and a lifetime of around 2 years (Novelli et al., 1999; Price et al., 2007; Xiao et al., 2007; Pieterse et al., 2011; 2013). H_2 can affect atmospheric chemistry and composition in several ways. Firstly, it increases the lifetime of the greenhouse gas methane (CH_4) via its competing reaction with the hydroxyl radical (OH) (Schultz et al., 2003; Warwick et al., 2004). Additionally, H_2 affects air quality because it is an ozone (O_3) precursor and indirectly increases the lifetime of the air pollutant carbon monoxide (CO) through competition for OH. In the stratosphere, H_2O that is produced through the oxidation of H_2 increases humidity, which can result in increased formation of polar

64 stratospheric clouds and O_3 depletion (Tromp, et al., 2003), but this effect may
65 be weaker than estimated initially (Warwick et al. 2004; Vogel et al., 2012).
66
67 The main sources of tropospheric H_2 are the oxidation of CH_4 and non-methane
68 hydrocarbons (NMHC) (48%), biomass burning (19%), fossil fuel combustion
69 (22%) and biogenic N_2 fixation in the ocean (6%) and on land (4%), while the
70 main sinks are soil uptake (70%) and oxidation by OH (30%) (Pieterse et al,
71 2013).
72
73 The biogenic soil sink of H_2 is the largest and most uncertain term in the global
74 atmospheric H_2 budget. Conrad and Seiler (1981) assumed that the soil uptake
75 of atmospheric H_2 is most likely due to consumption by abiotic enzymes, since
76 there were no soil microorganisms known to be able to fix H_2 at the low
77 atmospheric mole fraction at that time. This remained the basic hypothesis of
78 many further soil uptake studies (Conrad et al., 1983; Conrad and Seiler, 1985;
79 Ehhalt and Rohrer, 2011; Guo and Conrad, 2008; Häring et al., 1994; Smith-
80 Downey et al., 2006). However, Constant et al. (2008a) were first to identify an
81 aerobic microorganism (*Streptomyces* sp. PCB7) that can consume H_2 at
82 tropospheric ambient mole fractions, and suggested that active metabolic cells
83 could be responsible for the soil uptake of H_2 rather than extracellular enzymes.
84 Further studies showed that uptake activity at ambient H_2 level is widespread
85 among the streptomycetes (Constant et al., 2010) and it was postulated that high

affinity H_2-oxidizing bacteria are the main biological agent responsible for the soil uptake of atmospheric H_2 (Constant et al., 2011). Khdhiri et al. (2015) suggested that the relative abundance of high affinity H_2-oxidation bacteria and soil carbon content could be used as predictive parameters for the H_2 oxidation rate. Determining the dominant mechanism of the H_2 soil uptake activity is still an active area of research.

It has been shown that soil uptake of H_2 can coexist with soil production (Conrad, 1994). H_2 is produced in the soil during N_2 fixation (e.g. by bacteria living symbiotically in the roots of legumes such as clover or beans) and dark fermentation. Although the H_2 produced in the soil by e.g. N_2 fixation can be largely consumed within the soil, a significant amount of H_2 escapes to the atmosphere (Conrad and Seiler, 1979; 1980). Conrad and Seiler (1980) estimated that 2.4 to 4.9 Tg a^{-1} of H_2 is emitted into the atmosphere through N_2 fixation on land.

One approach to better understand the sources and sinks of H_2 is to investigate the isotopic fractionation processes involved, which act as a fingerprint for H_2 emitted from different sources or destroyed by different sinks. The isotopic composition of H_2 is expressed as:

$$\delta(\mathrm{D},\mathrm{H_2}) = \frac{R_{\mathrm{sa}}}{R_{\mathrm{VSMOW}}} - 1$$

107

108 where R_{sa} is the D/H ratio of the sample H_2 and R_{VSMOW} = (155.76±0.8) parts per
109 million (ppm = mmol mol^{-1}) is the same ratio of the standard material, Vienna
110 Standard Mean Ocean Water (VSMOW) (De Wit et al.,1980; Gonfiantini et al.,
111 1993). For brevity, we will use the notation δD (=δD(D, H_2)) throughout the
112 rest of this paper. The δD values are usually given in per mill (‰). Recent
113 studies showed that the global mean δD value of atmospheric H_2 is about +130 ‰
114 (Batenburg et al., 2011; Gerst et al., 2000, 2001; Rice et al., 2010).

115

116 The HH molecule is consumed preferentially over HD during both OH
117 oxidation and soil uptake, with OH oxidation causing a much stronger isotope
118 fractionation effect. Only a few studies have investigated the soil uptake of H_2
119 with isotope techniques. Gerst and Quay (2001) carried out field experiments in
120 Seattle, United States and found α_{soil} (= k_{HD}/k_{HH}) to be 0.943±0.024 (1σ). Note
121 that k_{HD} and k_{HH} are removal rate constants for HD and HH respectively. Rahn
122 et al. (2002a) collected air samples from four forest sites in ecosystems of
123 different ages in Alaska, United States, in July 2001, and obtained a similar
124 average value (0.94±0.01). They suggested that α_{soil} depends on the forest
125 maturity, with smaller fractionation for more mature forests. Since the more
126 mature forests showed larger deposition velocity (v_d) of H_2, they further

127 suggested that lower uptake rates involve greater isotopic fractionation (α_{soil}
128 further from 1) than fast uptake rates. Rice et al. (2011) performed deposition
129 experiments in Seattle and found α_{soil} varying from 0.891 to 0.976, with a mean
130 of 0.934. They found α_{soil} to be correlated with v_d, with smaller isotope effects
131 (α_{soil} closer to 1) occurring at higher v_d, which agreed with the suggestion by
132 Rahn et al. (2002a). In addition, unpublished experiments from Rahn et al.
133 (2005) yielded $\alpha_{soil} = 0.89 \pm 0.03$ in three upland ecosystems that were part of an
134 Alaskan fire chronosequence. The data suggest that variability in the
135 soil/ecosystem affects α_{soil} but no significant variability of α_{soil} with season was
136 detected. Hitherto, only α_{soil} values from studies in Seattle and Alaska are
137 available, and values from other locations and ecosystems are needed to learn
138 more about the factors influencing α_{soil}.
139
140 The δD of H_2 from various surface sources has been reported as about -290 ‰
141 for biomass burning (Gerst and Quay, 2001; Haumann et al., 2013) and between
142 -200 ‰ and -360 ‰ for fossil fuels combustion (Rahn et al., 2002b; Vollmer et
143 al., 2012). So far no field studies have determined the isotopic composition of
144 the H_2 emitted from soil. Two laboratory studies examined the isotopic
145 signature of H_2 produced from N_2 fixation. Luo et al. (1991) reported a
146 fractionation factor $\alpha_{H2/H2O} = R(D/H, H_2)/R(D/H, H_2O) = 0.448 \pm 0.001$ between
147 the H_2 produced from N_2 fixation and the H_2O used to grow the N_2-fixing
148 bacteria for *Synechococcus sp*. and 0.401±0.002 for *Anabaena sp*., respectively.

149 Walter et al. (2012) reported $\alpha_{H2/H2O}$ = 0.363±0.019 for the N_2-fixing
150 rhizobacterium *Azospirillum brasiliensis*. It has been proposed that
151 microbiological H_2 consumption and production could modify the thermal
152 isotopic equilibrium between H_2 and H_2O in low-temperature hydrothermal
153 fluids (Kawagucci et al., 2010). Compared to the surface sources, H_2 produced
154 from CH_4 and NMHC oxidation is isotopically strongly enriched in deuterium,
155 with δD beween +120 and +180 ‰ (Rahn et al., 2003; Röckmann et al. 2003a,
156 Pieterse et al., 2011).
157
158 Here we report measurements of the isotopic fractionation factors of H_2 during
159 soil deposition at two different sites in the Netherlands, a forest and a grassland
160 site. For the grassland site we also determine the apparent isotopic composition
161 of the H_2 that was simultaneously emitted from the soil during the experiment.
162
163
164 # 2. Methods
165
166 ## 2.1 Sampling
167
168 Air samples were collected from a soil chamber at two locations in the
169 Netherlands (Fig. 1): a grass field around the Cabauw tall tower (51°58' N,

4°55' E) and a forest site near Speuld (52°13' N, 5°39' E). Two types of ground cover (grass with and without clover) were sampled at Cabauw, while three types of forest (Douglas fir, beech and spruce) were selected in Speuld. More information about the soil and vegetation type can be found in Beljaars and Bosveld (1997) for the Cabauw site, and in Heij and Erisman (1997) for the Speuld site.

Flask samples were filled with air from a soil chamber, using a closed-cycle air sampler (Fig. 2). The soil chamber consisted of two parts: the chamber body with a metal base at the bottom that was inserted about 2 cm into the soil, and a removable transparent lid with two connections for air sampling. The chamber had a height of 40 cm, an area of 570 cm^2 and a volume of 22.8 L; the air inside was mixed by a fan. The sampler could hold four flasks installed in series, which could be bypassed independently; the flow and pressure in the flasks were controlled. The air was dried using $Mg(ClO_4)_2$. After passing through the flasks the air was returned to the soil chamber, which kept the pressure inside the chamber approximately constant during sampling.

Air samples were collected from the chamber in 1 L glass flasks at 0, 10, 20 and 30 minutes after closing the chamber (time interval changed to 5 minutes in Speuld because of the faster uptake). The gas flasks (Normag, Ilmenau, Germany) were made of borosilicate glass 3.3 with O-ring-sealed stopcocks

made of PCTFE (Kel-F) and covered with a dark hose. Thorough tests have demonstrated that air samples with typical trace gas content are stable in these flasks (Rothe et al., 2004). In the beginning, the whole sampling unit (all lines, connections and flasks) was flushed with ambient air for about 10 minutes at a flow rate of 2 L min^{-1} and a pressure of 100 kPa, with all flasks open and the chamber lid open. This initial flushing process was designed to fill the flasks with background air. The air pressure inside the flasks was increased to 200 kPa (180 kPa for Speuld samples) by adjusting the flow control valve and the valves on two pressure gauges (Fig. 2) before chamber closing and then maintained constant during the whole sampling time. The flow rate was maintained at 2 L min^{-1} at ambient pressure and temperature with a rotameter and the pressure inside the chamber was maintained at 100 kPa during the whole sampling time. The temperature was not recorded during the sampling. After the initial flushing, the first flask was closed and then the chamber was closed as well. Afterwards, the air was flushed from the chamber through three flasks (the first flask was by-passed) and back to the chamber. After 10, 20 and 30 minutes, the second, third and fourth flasks were closed.

A total of 36 sets of air samples were collected in Cabauw during summer (June, July and August) 2012 and 12 sets were collected in Speuld in September 2012. Each set contains four air samples. In total, 186 valid samples were analyzed for H_2 mole fraction and its deuterium content (6 were lost during sampling,

transportation and measurement). All the Speuld samples and about half of the Cabauw samples were further used for analysis in this study. The reason why 50% of the Cabauw experiments were not used is that these experiments showed neither strong H_2 emission nor H_2 uptake and the isotopic signals were weak. Most experiments were conducted with the 22.8 L volume soil chamber as described above, while 10 experiments were conducted with a larger automated soil chamber with a volume of 125 L and a height of 22.5 cm.

2.2 Laboratory determination of H_2 mole fraction and deuterium content of air samples

The mole fraction and the δD of H_2 were measured with a gas chromatography isotope ratio mass spectrometry (GC/IRMS) setup (Rhee et al., 2004). For H_2 mole fractions, the laboratory working standards are linked to the MPI-2009 scale (Jordan and Steinberg, 2011). The δD values of the laboratory reference gases are indirectly linked to mixtures of synthetic air with H_2 of known isotopic composition, certified by Messer Griesheim, Germany (Batenburg et al., 2011). Most of the samples collected from Cabauw were measured within two months after sampling, while the samples from Speuld were kept in a dark storage room for around four months before measurement.

The operational principle of the GC/IRMS system is to separate H_2 from the air matrix at low temperature (about 36 K) and measure the HH and HD content with a mass spectrometer. The measurement includes four main steps:

(1) A glass sample volume (750 ml) is evacuated and subsequently filled with sample air to approximately 700 mbar. This volume is then exposed to a cold head (36 K) of a closed-cycle helium compressor for 9 minutes. During this stage, all gases except H_2, helium (He) and neon (Ne) condense.

(2) The remainder in the headspace of the cold head and sample volume is then flushed with He carrier gas to a pre-concentration trap where H_2 is collected on a 25 cm long, 1/8 inch OD (outside diameter) stainless steel tube filled with fine grains (0.2 to 0.5 mm) of 5 Å molecular sieve, for 20 minutes. The pre-concentration trap is cooled down to the triple point of nitrogen (63 K) by keeping it in a liquid N_2 reservoir that is further cooled down by pumping on the gas phase.

(3) After the collection of H_2, the pre-concentration trap is warmed up to release the absorbed H_2, which is then cryo-focused for 4 minutes on a capillary (25 cm long, 0.32 mm ID (inside diameter)) filled with 5 Å molecular sieve at 77 K. After that, the cryo-focus trap is warmed up to ambient temperature and the H_2

sample is flushed with He carrier gas onto the GC column (5 Å molecular sieve, ≈323 K) where H_2 is chromatographically purified from potential remaining interferences.

(4) In the end, the purified H_2 is carried by the He carrier gas via an open split interface (Röckmann et al., 2003b) into the IRMS for D/H ratio determination.

More details about the GC/IRMS system and measurement steps can be found in Rhee et al. (2004) and Röckmann et al. (2010). The data correction procedures and isotope calibration are similar to those described in Batenburg et al. (2011). Four reference gases were used to determine the δD values of the samples. Two of them (Ref-1 and Ref-2) with δD values of (+207.0 ± 0.3) ‰ and (+198.2 ± 0.5) ‰ were calibrated and used previously in Batenburg et al. (2011). The other two new reference gases (Ref-3 and Ref-4) were calibrated versus Ref-1 and Ref-2. The δD value of Ref-3 was (-183± 2.4) ‰. Ref-4 was a frequently measured reference gas that was measured usually about 5 times per sequence of measurement, while other three reference gases were measured about 1 to 3 times per sequence of measurement. The δD value of Ref-4 dropped linearly with time from -115 ‰ to -157 ‰ between 1 Jun 2012 and 15 Feb 2013, while the other three reference gases were stable.

2.3 Non-linearity of the GC/IRMS system

Ideally, the δD of H_2 measured with the GC/IRMS should not depend on the total amount of H_2 used for analysis, but in practice a dependence of the isotopic composition on the amount of H_2 is observed for low mole fractions. This is called non-linear behavior, and it is a particularly severe limitation for soil uptake studies, since the mole fraction in such samples can decrease by more than an order of magnitude. For comparison, in ambient background air the H_2 mole fraction variations are usually no more than 20%.

Experiments were carried out with different quantities of air from various laboratory reference bottles with known δD to determine a suitable correction for the non-linear behavior. The measured δD increases with the mass 2 sample peak area, which is proportional to the H_2 quantity in the sample. In the peak area range of 0.2 Vs to 1 Vs this relation can be parameterized by a logarithmic function $\delta D = 54.6 \ln(\text{peak area/Vs})$ ‰, which is used as correction function for the measurements at low peak areas (Fig. 3). The linearity correction introduces an additional uncertainty due to uncertainties in the logarithmic fit, particularly at low peak areas. The total assigned uncertainty for each measurement is calculated from the analytical and fitting uncertainty, as a function of peak area (Fig. 4). It is 2 ‰ for ln (peak area/Vs) of 1.5 or more

(equivalent to more than 600 ppb H_2 in an air sample), but increases to 32 ‰ when ln (peak area/Vs) drops to -1.6 (≈ 20 ppb H_2 in air sample). In total, the δD results of 18 Speuld samples that were measured at these low peak areas were corrected with this linearity correction. Possible additional systematic errors (a few ‰) may arise from uncertainties in the initially assigned δD values of the commercial calibration gases, changes of these values in the process of creating calibration mixtures with near-ambient H_2 concentration, and the calibration measurements themselves (Batenburg et al., 2011).

2.4 Data evaluation

Assuming first order kinetics for H_2 removal and a constant production rate P over the course of a deposition experiment, the time evolution of the mole fraction c of non-deuterated H_2 (HH) inside the soil chamber can be expressed as:

$$\frac{\mathrm{d}\,c}{\mathrm{d}t} = P - kc \qquad (1)$$

where k is the first order uptake rate constant of HH. For well-mixed air in the chamber, $k = v_d/h$, where v_d is the gross deposition velocity of H_2 and h is the

319 chamber height. The gross deposition velocity is the deposition velocity
320 corrected for production, which is different from the net deposition velocity
321 reported in some studies in the past that showed the effective uptake of H_2 from
322 the atmosphere. The solution of Eq. (1) is of the form:
323

$$c = (c_{\mathrm{i}} - c_{\mathrm{e}})e^{-kt} + c_{\mathrm{e}} \qquad (2)$$

324
325 where c, c_{i} and c_{e} (= P/k) are the mole fractions of HH at time t, initially and at
326 equilibrium, respectively. Therefore, P and k can be obtained by fitting an
327 exponential function to the time evolution of HH inside the chamber. Similarly,
328 we can obtain P' and k' from the time evolution of HD.
329

$$c' = (c'_{\mathrm{i}} - c'_{\mathrm{e}})e^{-k't} + c'_{\mathrm{e}} \qquad (3)$$

330
331 where c', c_{i}', c'_{e} (= P'/k'), P' and k' are the corresponding parameters for HD.
332
333 Equations (2) and (3) constitute the mass balance model that we used to analyze
334 our data. When k, k', P and P' have been determined, α_{soil} and $\delta\mathrm{D}_{\mathrm{soil}}$ can be
335 calculated simply as:
336

$$\alpha_{\mathrm{soil}} = \frac{k'}{k} \qquad (4)$$

337

$$\delta D_{\mathrm{soil}} = \frac{P'/P}{2R_{\mathrm{VSMOW}}} - 1 \qquad (5)$$

338

339 However, fitting an exponential curve to only four sample data yields relatively
340 large errors for k, k', P and P', which propagate to large errors for α_{soil} and $\delta\mathrm{D}_{\mathrm{soil}}$
341 if they are determined directly from Eqs (4-5).

342

343 In Rice et al. (2011), Equations (2) and (3) were combined to calculate α_{soil} in
344 the presence of both source and sink of H_2 using c_e and c_e' from the exponential
345 fits:

346

$$\ln\frac{c' - c_e'}{c_i' - c_e'} = \frac{k'}{k}\ln\frac{c - c_e}{c_i - c_e} \qquad (6)$$

347

348 $\alpha_{\mathrm{soil}} = k'/k$ can be obtained by plotting $\ln\frac{c'-c_e'}{c_i'-c_e'}$ versus $\ln\frac{c-c_e}{c_i-c_e}$ and fitting a linear
349 function. In the absence of soil emission ($c_e = c'_e = 0$), Eq. (6) collapses to the
350 well-known Rayleigh fractionation equation that is used to quantify the isotope
351 fractionation during single stage removal processes in the absence of sources.

352

For the high emission measurements, where production overwhelms consumption, we use the relations $c_e = P/k$ and $c'_e = P'/k'$, and obtain P'/P from the slope of $c'_e \ln\frac{c'-c'_e}{c'_i-c'_e}$ against $c_e \ln\frac{c-c_e}{c_i-c_e}$. Then δD_{soil} is calculated from Eq. (5).

2.5 Flask sampling model

The advantage of sampling with the soil chamber system described in Section 2.1 was that the pressure in the soil chamber stayed constant even when several large samples (2 L each) were taken. A disadvantage was that the volume of air inside the flasks (8 L of air in total) was considerable compared to the volume of air inside the soil chamber (22.8 L). This had two effects: (1) A significant part of the air was at each time separated from the chamber and thus from the soil production and uptake. (2) Because of the time lag to flush the samples, the air in a flask was not the same as the air in the chamber at the same time.

We built a flask sampling model to derive correction factors that take into account the influence of the flask sampling system. For a given combination of uptake and production rates, the model simulates the evolution of the H_2 mole fraction in two configurations: the soil chamber alone, and the soil chamber plus four flasks as in our experiments. The model is described in detail in Appendix A. An example of a simulation is shown in Fig. 5. Compared to the situation

374 without flasks, there is a time lag in the decay of H_2 for both the chamber and
375 the flasks after introducing four flasks in the model. The time lag for the second
376 flask is about 2.5 minutes. It increases to 5 minutes for the third flask and is
377 even longer for the fourth flask.

378

379 It is obvious that the sampling process strongly affects the uptake rate k_{app} and
380 production rate P_{app} obtained from the direct flask measurements, so we
381 corrected all k_{app} and P_{app} values with the correction coefficients derived from
382 this flask sampling model (Appendix A). For a fixed chamber volume, sample
383 pressure, flow rate and time interval of the flask collection that are all recorded
384 for each experiment, the relationship between the actual uptake rate constant
385 k_{true} and apparent uptake rate constant k_{app} can be obtained (see Appendix A).
386 Under the same sampling conditions for a fixed value of P_{app}, the relationship
387 between actual production rate P_{true} and apparent production rate P_{app} depends
388 on k_{true} (Fig 10b).

389

390 To evaluate the data, we first applied an exponential fit as in Eq. (2) to the
391 measured HH mole fractions for the four flasks in each experiment and obtained
392 *apparent* values k_{app}, P_{app} and $c_{e,app}$ from the fit parameters. Then we used the
393 correction factors derived from the flask sampling model to retrieve true values

394 k_{true} and P_{true} from the apparent values k_{app} and P_{app}. One can obtain k'_{true} and P'_{true}
395 by applying the same method to HD mole fractions inside four flasks.
396
397 To determine α_{soil}, we plotted $\ln\frac{c'-c'_{e,app}}{c'_1-c'_{e,app}}$ versus $\ln\frac{c-c_{e,app}}{c_1-c_{e,app}}$ (Eq.6, Fig. 7) and
398 obtained $\alpha_{soil,app}$ from the slope of the linear regression. Here, c and c' are HH
399 and HD mole fractions in each of the four flasks; c_1 and c'_1 are HH and HD
400 mole fractions of the first flask; $c_{e,app}$ and $c'_{e,app}$ are apparent HH and HD
401 equilibrium mole fractions obtained from the exponential fits of HH and HD
402 mole fractions inside the four flasks. We determined the relationship (Fig. 10c)
403 between $\alpha_{soil,true}$ and $\alpha_{soil,app}$ obtained from $\ln\frac{c'-c'_{e,app}}{c'_1-c'_{e,app}}$ versus $\ln\frac{c-c_{e,app}}{c_1-c_{e,app}}$ using the
404 flask sampling model (see Appendix A1.3). The correction coefficients for each
405 experiment are given in Table 3.
406
407 Similarly, we obtained P'_{app}/P_{app} by plotting $c'_{e,app}\ln\frac{c'-c'_{e,app}}{c'_1-c'_{e,app}}$ versus
408 $c_{e,app}\ln\frac{c-c_{e,app}}{c_1-c_{e,app}}$ (Fig. 9), and calculated $\delta D_{soil,app}$ by use of Eq. (5). Then we
409 retrieved $\delta D_{soil,true}$ by use of the flask sampling model (Fig. 10d). The
410 corresponding correction coefficients for $\delta D_{soil,app}$ for each net-emission
411 experiment are shown in Table 3. More information about the retrievals of
412 $\alpha_{soil,true}$ and $\delta D_{soil,true}$ can be found in Appendix A.
413

414 Overall, the sampling effect on δD_{soil} is small (less than 22‰). This means that
415 the flask sampling system strongly affects the temporal evolution of HH and
416 HD individually (Fig. 5), and the uptake and production rates derived from flask
417 measurements, but the effects on the computed isotopic signature of the source
418 and sink are relatively small. More details and discussion of the flask sampling
419 model corrections are provided in Appendix A.
420
421
422 # 3. Results
423
424 ## 3.1 Temporal evolution of H_2, HD and δD
425
426 Fig. 6 shows examples for the temporal evolution of H_2, HD and δD in Cabauw
427 and Speuld, with error estimates included. The errors for H_2 and HD are about 4%
428 of the respective mole fraction. The error for δD ranges from 2 ‰ to 17 ‰.
429
430 Some of our Cabauw experiments show net soil emission of H_2 (upper panels)
431 and some show net soil uptake (middle panels), while all Speuld experiments
432 show net uptake of H_2 (lower panels). In the Cabauw net emission experiments,
433 the increase in H_2 mole fractions is associated with a strong decrease in δD,
434 showing a strongly depleted H_2 source. However, the net uptake experiments at

Cabauw show also a decrease in δD, albeit smaller. In the Speuld experiments, the uptake of H_2 is much faster; the δD increases in the beginning but then decreases again towards the end of the sampling, when the H_2 mole fractions are low.

As mentioned in the introduction, soil uptake tends to increase δD while soil emission tends to decrease δD of H_2. The continuous decrease of δD with time in all Cabauw experiments and the eventual decrease of δD in all Speuld experiments clearly show that there is concurrent soil emission even with net uptake. Thus, the equilibrium H_2 concentration in our experiments is not just a threshold concentration where microbial uptake stops, but the isotopic evolution shows that there is an active overlapping emission (Conrad, 1994).

3.2 Emission and uptake strength of H_2

The production rate $P = P_{true}$ and uptake rate constant $k = k_{true}$ were obtained by applying exponential fits to the temporal evolution of H_2, and applying the corrections derived from the flask sampling model (appendix A) to the P_{app} and k_{app} obtained from the exponential fits (Fig. 6). The deposition velocity (v_d),

455 production flux (F_p), initial uptake flux (F_u) and net flux at the beginning of the
456 experiment (F_n) were then calculated as follows:
457

$$v_d = kh \qquad (7)$$

458

$$F_p = \frac{Ph}{V_M} \qquad (8)$$

459

$$F_u = \frac{kc_1h}{V_M} \qquad (9)$$

460

$$F_n = F_p - F_u \qquad (10)$$

461

462 where h, V_M and c_1 are the chamber height, standard molar volume (=22.4 L
463 mol^{-1}) and H_2 mole fraction of the first flask, respectively. We note that with our
464 method we derive v_d as deposition velocity for the gross uptake, unlike most of
465 the results reported in the literature that just measured net uptake.
466
467 The strongest soil uptake occurs in the Speuld experiments (Table 1a), with a
468 mean v_d of (0.17±0.02) (2 SE, n=12) cm s^{-1} (SE represents standard error). On
469 average, the Cabauw experiments show weaker soil uptake, with a mean v_d of
470 (0.13±0.06) (2 SE, n=8) cm s^{-1} for the net-uptake experiments (Table 1b) and

(0.06±0.03) (2 SE, n=9) cm s^{-1} for the net-emission experiments (Table 2). In terms of the net H_2 flux F_n, this is (-26.5±4.8) (2 SE, n=12) nmol m^{-2} s^{-1} for Speuld experiments (Table 1a), (-13.6±8.6) (2 SE, n=8) nmol m^{-2} s^{-1} for Cabauw net-uptake experiments (Table 1b) and (49.5±29.8) (2 SE, n=9) nmol m^{-2} s^{-1} for Cabauw net-emission experiments (Table 2), indicating strong uptake, weaker uptake and strong emission of H_2, respectively.

3.3 Fractionation during soil uptake

Soil uptake and soil emission have opposite effects on the isotopic composition of H_2 and can partly cancel each other. This will lead to additional uncertainty and we expect to obtain the most robust fractionation factor for soil uptake when the soil uptake is larger than the soil emission (Table 1a&b).

The resulting α_{soil} for Speuld (Table 1a) varies from 0.913 to 0.955, with a mean value of 0.937±0.008 (2 SE, n=12). Error estimates for HH and HD mole fraction at time t and at equilibrium are considered for the final error estimates of α_{soil} for each experiment.

Table 1b shows α_{soil} of the Cabauw net-uptake experiments. It should be noted that the soil emitted H_2 interferes much more with the fractionation during uptake in these Cabauw net-uptake experiments than for the Speuld experiments, which is illustrated by the consistent decrease in δD in the middle panel of Fig. 6. The derived values for α_{soil} vary from 0.911 to 1.019 with a mean value of 0.951±0.026 (2 SE, n=8) for these 8 selected Cabauw net-uptake experiments. Both the mean and the standard error are higher than for the Speuld experiments (0.937±0.008), but the difference is not significant at the 0.1 confidence level.

To graphically illustrate the calculation of α_{soil} with the mass balance model, we plot $\ln\frac{c'-c'_{e,app}}{c'_1-c'_{e,app}}$ versus $\ln\frac{c-c_{e,app}}{c_1-c_{e,app}}$ for all Speuld and Cabauw net-uptake experiments in Fig. 7. A linear fit is applied to all the data and the overall $\alpha_{soil,app}$ is found to be 0.947±0.004 (95% CI). Applying a correction factor is not straightforward now because this analysis combines the results from different experiments. If we use the average of $\alpha_{soil,true}/\alpha_{soil,app}$ ratios (0.998) for all net-uptake experiments in Table 3 as the correction coefficient for this overall $\alpha_{soil,app}$, the overall α_{soil} is 0.945±0.004 (95% CI).

Fig. 8 shows α_{soil} as a function of v_d for all Speuld experiments and Cabauw net-uptake experiments. The R^2 value is nearly zero and the p-value is 0.53 for the linear regression of all experiments, so no significant correlation between α_{soil}

512 and v_d is found. Also, no significant correlation is found when considering the
513 Speuld and Cabauw net-uptake experiments separately.
514
515
516 **3.4 Isotopic signature of H_2 emitted from soil**
517
518 As discussed in Section 2.4, the isotopic signature of H_2 emitted from the soil
519 (δD_{soil}) can be obtained from the mass balance model. In order to minimize the
520 influence of soil uptake on the computed δD_{soil} and obtain the most robust result,
521 we only consider the Cabauw experiments with strong soil emission and weak
522 soil uptake ($c_{e,app} > 1500$ ppb). In total, 9 Cabauw experiments are selected
523 (Table 2) and a linear fit is applied to the plot of $c'_{e,app} \ln \frac{c'-c'_{e,app}}{c'_1-c'_{e,app}}$ versus
524 $c_{e,app} \ln \frac{c-c_{e,app}}{c_1-c_{e,app}}$ for each experiment (Fig. 9). It can be seen that the linear
525 function fits the data very well for each experiment. The slope of the linear fit
526 yields P'_{app}/P_{app}. This P'_{app}/P_{app} ratio is used to calculate $\delta D_{soil,app}$ (Eq. (5)). After
527 correcting for the flask sampling effects (see Appendix A), the corresponding
528 δD_{soil} values are shown in Table 2. The δD_{soil} value ranges from -629 ‰ to -
529 451 ‰, with a mean value of (-530±40) ‰ (2 SE, n=9), which is very D-
530 depleted, but still considerably enriched relative to the value around -700 ‰
531 expected for thermodynamic equilibrium between H_2 and H_2O (Bottinga, 1969).

4. Discussion

4.1 Emission and uptake strength of H_2

The deposition velocity v_d is a measure of the strength of soil uptake. Both microbial removal and diffusion can affect v_d, and they can both be influenced by the temperature and moisture content of the soil (Ehhalt and Rohrer, 2013a; 2013b). On average, the v_d obtained in this study is larger in the forest region (Table 1a) than in the grass/clover region (Table 1b and 2), in agreement with the conclusion from Ehhalt and Rohrer (2009).

The v_d of (0.06±0.03) cm s^{-1} found in our Cabauw net-emission experiments (Table 2) is similar to those reported in Conrad and Seiler (1980) (0.07 cm s^{-1}, both grass and clover) and Gerst and Quay (2001) (0.04 cm s^{-1}, grass), while the v_d of (0.13±0.06) cm s^{-1} in Cabauw net-uptake experiments (Table 1b) is larger than those studies with similar soil cover but close to values of 0.12 to 0.14 cm s^{-1} found in savanna soil (Conrad and Seiler, 1985). The stronger soil uptake in Speuld forest ((0.17±0.02) cm s^{-1}) agrees well with the beech forest results (0.06 to 0.22 cm s^{-1}) in Förstel (1988) and Förstel and Führ (1992). However, other

553 studies at forest sites cited in Ehhalt and Rohrer (2009) showed lower v_d than
554 our Speuld results. We note here that the v_d values reported in Conrad and Seiler
555 (1980; 1985) were gross deposition velocities while those reported in Gerst and
556 Quay (2001) were net deposition velocities. The specific method used to obtain
557 v_d was not documented in the other studies. v_d obtained from our experiments
558 are gross deposition velocities.
559
560 The net uptake flux F_n in our Speuld experiments and Cabauw net-uptake
561 experiments is much larger than those found in Smith-Downey et al. (2008).
562 They found a F_n of about -8 nmol m^{-2} s^{-1} for the forest, desert, and marsh, which
563 was similar to that for loess loamy soil in Schmitt et al. (2009). Our results are
564 within the F_n range found in the mixed wood plains by Constant et al. (2008b)
565 and the Harvard forest by Meredith (2012). Previously at our Cabauw site, Popa
566 et al. (2011) obtained a F_n of only -3 nmol m^{-2} s^{-1} by using the radon tracer
567 method. However, the Cabauw net-uptake experiments used for this evaluation
568 were from selected places where uptake was strong, while the results in Popa et
569 al. (2011) represented the overall uptake in the footprint of the Cabauw site,
570 which is a much larger area (tens of km^2).
571
572 Khdhiri et al. (2015) performed microbiological analyses on soil samples from
573 the Cabauw and Speuld sites, in order to find the drivers of soil H_2 uptake. They
574 observed that the H_2 uptake rate under standard incubation conditions was

575 significantly lower for the Cabauw soil samples than for the Speuld ones, which
576 is consistent with our findings. The main factors that explained the differences
577 were the relative abundance of high affinity H_2-oxydizing bacteria and the soil
578 carbon content, both lower on average for the Cabauw site.
579
580 The emission of H_2 from the soil is large for the Cabauw net-emission
581 experiments, with F_n ranging from 13.7 to 150.2 nmol m^{-2} s^{-1} and a median
582 value of 41.0 nmol m^{-2} s^{-1} (Table 2). One experiment, "CBW-28", shows
583 unusually high emission, with H_2 increasing to 3010 ppb within 30 minutes. In
584 comparison, Conrad and Seiler (1980) found a F_n of 23-32 nmol m^{-2} s^{-1} for a
585 clover field. Except for the experiments "CBW-28" and "CBW-31", our
586 Cabauw net-emission experiments are close to the F_n found by them. The
587 variability in F_n could be attributed to different N_2 fixation flux in our
588 experiments, which could be affected by both spatial density of N_2 fixation
589 organisms and their N_2 fixation activities. The N_2 fixation activity could be
590 regulated by various factors including temperature, moisture, light availability
591 and carbon storage etc. (Belnap, 2001), which were not measured are therefore
592 not discussed here.
593
594

595 ## 4.2 Fractionation during soil uptake

596

597 Fractionation during soil uptake of H_2 can happen during the diffusion into the
598 soil and due to microbial removal within the soil. To further investigate the
599 factors determining α_{soil}, information about the soil cover is provided in Table
600 1a&b. It is evident that no large differences exist between the Douglas fir,
601 spruce and beech sites, i.e. the variability between sites is similar to the
602 variability within sites. The small number of experiments impedes examining
603 the possible small differences between sites. In order to investigate the diffusion
604 effect, we removed the soil cover in experiments "SPU-8" and "SPU-12" at the
605 same place of experiments "SPU-7" and "SPU-11". The removal of leaves
606 ("SPU-8") and needles ("SPU-12") increased α_{soil} by $\approx$ 0.014, thus towards
607 smaller fractionation, which indicates that diffusion contributes to the
608 fractionation. As v_d also increases when the soil cover is removed, faster
609 deposition is associated with smaller fractionations in these experiments, which
610 is similar to the results from Rice et al. (2011).

611

612 The α_{soil} for the Cabauw net-uptake experiments is higher and more scattered
613 than that for the Speuld experiments (0.951±0.026 vs. 0.937±0.008). This could
614 be caused by the interference of D-depleted H_2 from the strong soil emission in
615 Cabauw, which may not be perfectly captured via the mathematical models
616 applied. As can be seen from the strong decline of δD with time in the middle
617 panel of Fig. 6, though soil uptake of H_2 dominates for the Cabauw net-uptake

618 experiments, soil production is still considerable. If part of the source signature
619 is not taken into account properly and appears in α_{soil}, then α_{soil} will be larger,
620 because soil production tends to decrease δD of H_2. This could explain why α_{soil}
621 is even larger than 1 in "CBW-7".
622
623 The overall α_{soil} (0.945) obtained by plotting $\ln\frac{c'-c'_{e,app}}{c'_1-c'_{e,app}}$ versus $\ln\frac{c-c_{e,app}}{c_1-c_{e,app}}$ and
624 applying the average correction factor for all the Speuld and Cabauw net-uptake
625 experiments is similar to the results of 0.943±0.024 from Gerst and Quay (2001)
626 and 0.94±0.01 from Rahn et al. (2002a). They suggested that the overall α_{soil} is
627 more accurate as it is less susceptible to outliers. We argue here that the average
628 α_{soil} of all individual experiments in Speuld (0.937) and Cabauw (0.951) is
629 representative for a spatially averaged fractionation factor for those sites and is
630 useful for e.g. characterizing the phenomenon and comparing with other
631 fractionation results. If all experiments are included in one fit, their weight for
632 determining the slopes depends on how much H_2 has been removed, so
633 experiments with a lower $c_{e,app}$ have a larger weight than experiments with a
634 higher $c_{e,app}$ (i.e. experiments with a higher v_d have a larger weight than
635 experiments with a lower v_d). The fractionation factor obtained by fitting all
636 data together is therefore representative for a flux weighted average, which is
637 the relevant number for the global atmospheric isotope budget.
638

4.3 Relationship between α_{soil} and v_d

Rice et al. (2011) proposed a significant positive correlation between α and deposition velocity v_d in their soil uptake experiments. Fig. 8 shows that no significant correlation between α_{soil} and v_d is found when considering all Speuld and Cabauw net-uptake experiments. The uptake rate is much stronger in the Speuld experiments ($v_d \approx 0.17$ cm s^{-1}) than in the study of Rice et al. (2011) ($v_d \approx 0.04$ cm s^{-1}), but the α_{soil} is virtually identical (0.937 *versus* 0.934). Therefore, when the results from both studies are combined, the correlation reported in Rice et al. (2011) between α_{soil} and v_d disappears. We suggest that a positive correlation between α_{soil} and v_d may exist for a specific site where microbial species are similar. This was suggested from the simultaneous increase of both α_{soil} and v_d in two experiments ("SPU-8" and "SPU-12"), when soil cover was removed at the same sampling location, as mentioned in Section 4.2.

We conclude that there is certainly not one single correlation between α_{soil} and v_d that holds globally and the soil type might play an important role. Measurements at more sites may be needed to positively confirm whether local positive correlations between α_{soil} and v_d are common.

4.4 δD of H_2 emitted from the soil

The present study is the first field study to report δD of H_2 emitted from soils. The δD_{soil} values (-629 ‰ to -451 ‰) shown in Table 2 are less depleted than the H_2 in isotopic equilibrium with water (≈-700 ‰). Previous observations from environmental H_2 production yielded a δD of -628 ‰ for two seawater samples (Rice et al., 2010), -778 ‰ for a termite headspace sample and -690 ‰ for two headspace samples from a eutrophic water pond (Rahn et al., 2002b). Kawagucci et al. (2015) proposed that microbiological H_2 consumption and production could destroy the thermal isotopic equilibrium between H_2 and H_2O in low-temperature hydrothermal fluids. Luo et al. (1991) and Walter et al. (2012) found fractionation factors of 0.448, 0.401 and 0.363 for H_2 generated from water by different N_2-fixing bacteria in the laboratory.

In order to compare our δD_{soil} with the fractionation factors between H_2 and H_2O found by Luo et al. (1991) and Walter et al. (2012), we converted their fractionation factors to $\delta D(H_2)$ by assuming the $\delta D(H_2O)$ to be the same as that of global rainwater (-37.8 ‰, Hoffmann et al., 1998). This results in $\delta D(H_2)$ values of -651 ‰ to -569 ‰ for their N_2-fixing bacteria. Although the ranges are considerable, it appears that the mean δD_{soil} (-530 ‰) obtained in our field

680 study is even higher than what was found for nitrogenase-derived H_2 in
681 laboratory experiments.
682
683 It is known that H_2 produced by biogenic N_2 fixation can be largely recycled
684 within the soil before entering the atmosphere (Evans et al., 1987; Conrad and
685 Seiler, 1979; 1980). If this uptake process within the soil tends to increase the
686 δD of the remaining H_2, as the soil uptake process for atmospheric H_2 does, then
687 the H_2 entering the atmosphere will be less D-depleted than pure biogenic H_2.
688 However, if the fractionation factor of removal in the soil is similar to that
689 determined from the net-uptake experiments (≈0.94), a large fraction of H_2
690 needs to be removed in the soil before release to explain the D-enriched δD_{soil}
691 compared to the values reported in the literature.
692
693 The deuterium enrichment in the emitted H_2, compared to the value expected in
694 isotopic equilibrium with water, could also be caused by different fractionations
695 induced by different enzymes and/or a potentially enriched deuterium content of
696 the substrate water available for H_2 production in Cabauw. H_2 is generated from
697 the reduction of hydrogen ions (H^+ or D^+) in intracellular water (Yang et al.,
698 2012). It was found that the isotopic composition of intracellular water can be
699 different from that of extracellular water due to metabolic processing (Kreuzer-
700 Martin et al., 2006). Due to the differences in H-bonding and hydrogen ion

transport, the fractionation may be different for different microbe species, which could result in different isotopic signatures of the produced H_2. Measurements of the isotopic composition of produced H_2 may be a tool to investigate such effects.

Finally, we note that if our Cabauw net-emission experiments are analyzed with a simple Keeling plot approach (i.e. without considering uptake), the y axis intercept is -703 ‰. We know from the temporal evolution of H_2, HD and δD that this model is not adequate and that uptake was significant in our experiments, so a simple Keeling plot analysis can be misleading if uptake is not considered.

5. Conclusions

This study investigated the isotope effects associated with the production and uptake of atmospheric H_2 by soil. Our aim was to quantify the fractionation factor α_{soil} for H_2 deposition and the isotopic signature of H_2 emitted from the soil (δD_{soil}) from experiments carried out at Speuld and Cabauw.

721 The experiments covered a wide range of conditions from situations with very
722 strong net H_2 uptake to situations with very strong net H_2 emission. The
723 superposition of deposition and production made the analysis with simple
724 models like Rayleigh plot and Keeling plot impossible. Therefore, the mass
725 balance model suggested by Rice et al. (2011) was used for evaluation.
726
727 The deposition velocity v_d was largest in the Speuld experiments ((0.17±0.02)
728 cm s^{-1}) where also the strongest net soil uptake occurred, followed by the
729 Cabauw net-uptake experiments ((0.13±0.06) cm s^{-1}) and Cabauw net-emission
730 experiments ((0.06±0.03) cm s^{-1}). The net H_2 flux F_n was (-26.5±4.8) nmol m^{-2}
731 s^{-1} for Speuld experiments, (-13.6±8.6) nmol m^{-2} s^{-1} for Cabauw net-uptake
732 experiments and (49.5±29.8) nmol m^{-2} s^{-1} for Cabauw net-emission
733 experiments.
734
735 The mean fractionation factors α_{soil} are 0.937±0.008 for the Speuld forest soil
736 experiments and 0.951±0.026 for the Cabauw grassland experiments, which are
737 representative for a spatial average and useful for comparisons with other
738 fractionation studies. The Cabauw results may be affected by the relatively
739 strong concomitant soil emissions. The overall α_{soil} by considering all net-
740 uptake experiments is 0.945±0.004, which is representative for a flux weighted
741 average and useful for global isotope budget estimates. The fractionation factors
742 found in this work are in good agreement with previous studies.

743

744 No significant correlation between α_{soil} and deposition velocity v_d was found
745 while considering all of our experiments. The v_d were overall much larger in our
746 study than those in Rice et al. (2011) and we obtained similar values for α_{soil}.
747 This demonstrates that the positive correlation that was found previously does
748 not hold globally. From two of our Speuld experiments, α_{soil} increased after the
749 removal of leaves or needles above the soil. This indicates that there may be a
750 fractionation associated with diffusion through the surface layer of leaves or
751 needles during soil uptake, but more experiments are required to confirm this.

752

753 The isotopic analysis clearly showed that the net uptake was always a
754 superposition of a larger gross uptake and a gross emission flux. In Cabauw, the
755 emission strength was very large at locations where clover was present. Using a
756 simple mass balance approach, the isotopic composition of the emitted H_2 was
757 determined to be (–530±40) ‰, which is significantly higher than the value
758 expected for H_2O – H_2 isotope equilibrium. Although limited, other published
759 data on H_2 produced biologically via nitrogenase show also a tendency to more
760 enriched values. An additional isotope enrichment in our field soil study could
761 originate from fractionation during the recycling of H_2 within the soil before it
762 enters the atmosphere.

763

Appendix A

A1. Flask sampling model

A mathematical model is used to simulate the sampling and to correct for the effects of the flask sampling method on the values of uptake rate constant (k), production rate (P), fractionation factor (α_{soil}) and isotopic signature of H_2 produced from soil (δD_{soil}). We start with a pair of known (*true*) uptake and production rates and simulate the evolution of the mole fractions of H_2 and HD in the flasks and chamber. From the modeled mole fractions we calculate the *apparent* uptake and production rates and derive the correction needed to obtain the *true* uptake and production rates from measurement of the *apparent* rates in actual experiments.

A1.1 Mathematical description of the flask sampling model

The sampling setup is shown in Fig. 2 of the main paper. After 10 minutes of flushing, the chamber and the flasks contain ambient air with the prevailing H_2 and HD mole fractions. In the following we denote $c_1(t)$, $c_2(t)$, $c_3(t)$, $c_4(t)$ and $c_0(t)$ the H_2 mole fractions for the first, second, third, forth flask and the chamber, respectively. The moment when the first flask and the chamber lid are

785 closed is considered the starting time of the experiment (t=0). From this point
786 on, only the chamber, the second, third and fourth flask are connected, and the
787 initial H_2 mole fraction inside them is $c_0(0) = c_2(0) = c_3(0) = c_4(0) = c_1$. We start
788 a simulation with an input uptake rate constant (k_{true}) and an input production
789 rate (P_{true}). The simulation of the flask sampling is based on Eqs. (A1)-(A4)
790 shown below.
791
792 Assuming that the air in each flask and in the chamber is well-mixed during the
793 entire sampling process, the time evolution for the second flask $c_2(t)$, the third
794 flask $c_3(t)$, the forth flask $c_4(t)$ and the chamber $c_0(t)$ in the first 10 minutes after
795 starting the experiment can be expressed as:
796

$$\frac{\mathrm{d}c_2(t)}{\mathrm{d}t} = \frac{f}{V}c_0(t) - \frac{f}{V}c_2(t) \qquad \text{(A1)}$$

797

$$\frac{\mathrm{d}c_3(t)}{\mathrm{d}t} = \frac{f}{V}c_2(t) - \frac{f}{V}c_3(t) \qquad \text{(A2)}$$

798

$$\frac{\mathrm{d}c_4(t)}{\mathrm{d}t} = \frac{f}{V}c_3(t) - \frac{f}{V}c_4(t) \qquad \text{(A3)}$$

799

$$\frac{\mathrm{d}c_0(t)}{\mathrm{d}t} = \frac{f}{V'}c_4(t) - \frac{f}{V'}c_0(t) + (P_{\text{true}} - k_{\text{true}}c_0(t)) \qquad \text{(A4)}$$

800

where V and V' are the air volumes of the flask and chamber, and f is the flow rate. These differential equations are solved using the Matlab ODE solvers at time steps of 0.01 min. The input parameters are $c_0(0)$, P_{true}, k_{true}, V, V' and f. For each time step the solvers calculate the hydrogen flux into and out of the chamber and each flask, as well as the new mole fractions there.

After 10 minutes, the second flask is closed and now contains air with mole fraction $c_2 = c_2(10\text{ min})$. From this point on, only the chamber, the third and the fourth flask are connected, and the time evolution of the mole fractions can be expressed as:

$$\frac{\mathrm{d}c_3(t)}{dt} = \frac{f}{V}c_0(t) - \frac{f}{V}c_3(t) \qquad \text{(A5)}$$

$$\frac{\mathrm{d}c_4(t)}{dt} = \frac{f}{V}c_3(t) - \frac{f}{V}c_4(t) \qquad \text{(A6)}$$

$$\frac{\mathrm{d}c_0(t)}{dt} = \frac{f}{V'}c_4(t) - \frac{f}{V'}c_0(t) + (P_{\text{true}} - k_{\text{true}}c_0(t)) \qquad \text{(A7)}$$

After another 10 minutes of sampling, the third flask is closed $c_3 = c_3(20\text{ min})$, and only the chamber and the fourth flask are connected. Then, the time evolution for the fourth flask and the chamber can be expressed as:

$$\frac{\mathrm{d}c_4(t)}{dt} = \frac{f}{V}c_0(t) - \frac{f}{V}c_4(t) \qquad \text{(A8)}$$

$$\frac{\mathrm{d}c_0(t)}{dt} = \frac{f}{V'}c_4(t) - \frac{f}{V'}c_0(t) + (P_{\mathrm{true}} - k_{\mathrm{true}}c_0(t)) \qquad \text{(A9)}$$

The H_2 mole fraction inside the chamber and the fourth flask at time t=30 minutes is $c_0(30)$ and $c_4(30)$.

In the end, a set of four flasks with mole fractions $c_1(0)$, c_2(10 min), c_3(20 min) and c_4(30 min) is obtained. By fitting this set of four data points with an exponential function $\mathrm{c} = \mathrm{a}e^{-k_{\mathrm{app}}t} + c_{\mathrm{e,app}}$ (see Eq. (2) in the main paper), we can obtain the *apparent* soil uptake rate constant (k_{app}) and equilibrium concentration ($c_{\mathrm{e,app}}$) and further calculate *apparent* production rate (P_{app}=$k_{\mathrm{app}}c_{\mathrm{e,app}}$). These apparent rates k_{app} and P_{app} are different from the assumed *true* rates k_{true} and P_{true}. The flask sampling model enables us to establish a relation between k_{app} and P_{app} and k_{true} and P_{true}, so that k_{true} and P_{true} can be derived from k_{app} and P_{app} in actual experiments, where the true values are unknown. To accomplish this, simulations are carried out with a wide range of values for k_{true} and P_{true}, and a corresponding dataset of k_{app} and P_{app} is generated.

Similarly, we use a new set of input uptake rate constant k'_{true} and production rate P'_{true} for HD, and generate a corresponding dataset of k'_{app} and P'_{app}.

A1.2 The correction coefficients for *k* and *P*

Here we discuss an example of the relationship between k_{true} and k_{app} for the setup used in some Cabauw experiments (V'=22.8 L, f=2 L min^{-1} and Δt=10 min). The pressure inside the flasks is 200 kPa and the pressure inside the chamber is 100 kPa. The relationship between $k_{\mathrm{true}}/k_{\mathrm{app}}$ and k_{app} is shown in Fig. 10a. The ratio $k_{\mathrm{true}}/k_{\mathrm{app}}$ varies between 1.45 to 1.61 for our k_{app} range of 0.04 to 0.30 min^{-1}. This relationship does not depend on P_{true} (with P_{true} varying from 50 to 650 ppb min^{-1}). An additional uncertainty can arise from incorrect timing of the flask sampling, but sampling times should be correct within few seconds, which may lead to an additional uncertainty of below 1%. The uncertainty of the flow rate obtained from the rotameter due to variations in ambient pressure and temperature that were not recorded is less than 4%, and the effect on the ratio $k_{\mathrm{true}}/k_{\mathrm{app}}$ ratio is below 1%. We can retrieve k_{true} by multiplying k_{app} with the modeled value of $k_{\mathrm{true}}/k_{\mathrm{app}}$ for each experiment. The ratio $k_{\mathrm{true}}/k_{\mathrm{app}}$ for each experiment is shown in Table 3. It depends on experimental setup and k_{app} of each experiment, with a range of 1.177 to 1.589.

After retrieving k_{true} from k_{app}, we investigate the relationship between P_{true}/P_{app} and P_{app} for a fixed value of k_{true} (Fig. 10b). The ratio P_{true}/P_{app} depends slightly on P_{app} and k_{true}, ranging from 1.40 to 1.59 for a wide P_{app} range of 30 to 450 ppb min^{-1} and a wide k_{true} range of 0.05 to 0.45 min^{-1}. As for the correction of k, uncertainties arising from incorrect timing of the flask sampling and from pressure and temperature variations and their effect on the flow rate lead to additional uncertainties of P_{true}/P_{app} ratio below 1%, which are not considered. We can retrieve P_{true} by multiplying P_{app} with P_{true}/P_{app} for each experiment after having determined k_{true} from k_{app}. The ratio P_{true}/P_{app} for each experiment is shown in Table 3 and depends on the experimental setup, P_{app} and k_{app} of each experiment. It ranges from 1.152 to 2.759 for most experiments, with an exception of 7.472 for experiment SPU-2 where a very small P_{app} of 0.67 ppb min^{-1} is found. Although the ratio P_{true}/P_{app} of experiment SPU-2 is high, P_{true} of SPU-2 is still smaller than the rest of the experiments. P_{true}/P_{app} ratios for experiments SPU-10 and SPU-11 are null because these two experiments show a P_{app} of zero.

A1.3 The correction coefficients for α_{soil} and δD_{soil}

In our experiments, the uncertainties of k_{app} and k'_{app} derived from exponential fits to the time evolution of HH and HD are rather large, which results in a large scatter of $\alpha_{soil,app}$ if $\alpha_{soil,app}$ is calculated directly as k'_{app}/k_{app}. Thus, we obtained

878 $\alpha_{soil,app}$ by plotting $\ln\frac{c'-c'_{e,app}}{c'_1-c'_{e,app}}$ versus $\ln\frac{c-c_{e,app}}{c_1-c_{e,app}}$ (Fig. 7) for each experiment

879 which yields a smaller scatter for $\alpha_{soil,app}$.

880

881 Correction coefficients to convert $\alpha_{soil,app}$ to $\alpha_{soil,true}$ are obtained using the flask

882 sampling model by comparing $\alpha_{soil,true}$ used as input for the model run to $\alpha_{soil,app}$

883 derived from the plot of $\ln\frac{c'-c'_{e,app}}{c'_1-c'_{e,app}}$ versus $\ln\frac{c-c_{e,app}}{c_1-c_{e,app}}$ of the output values, like

884 in the experiments. Fig. 10c shows $\alpha_{soil,true}/\alpha_{soil,app}$ as a function of $\alpha_{soil,app}$ for a

885 wide $\delta D_{soil,true}$ range of -750‰ to -250‰ with the sampling setup described

886 above (V'=22.8 L, f=2 L min^{-1} and Δt=10 min) for k_{true}=0.25 min^{-1} and P_{true}=50

887 ppb min^{-1}. In this case the correction factor $\alpha_{soil,true}/\alpha_{soil,app}$ varies from 0.98 to

888 1.00 for a $\alpha_{soil,app}$ range of 0.90 to 1.00, and it does not depend on $\delta D_{soil,true}$. Thus,

889 after retrieving k_{true} and P_{true} as described in Section A1.2, we can retrieve $\alpha_{soil,true}$

890 from $\alpha_{soil,app}$ for each experiment. The correction factors range from 0.984 to

891 1.007, depending on the experimental setup and $\alpha_{soil,app}$ of each experiment

892 (Table 3).

893

894 Similarly, in our experiments, the uncertainties of P_{app} and P'_{app} derived from

895 exponential fits of time evolution of HH and HD are large, which results in a

896 large scatter of $\delta D_{soil,app}$ if $\delta D_{soil,app}$ is calculated directly from these P'_{app} and P_{app}.

897 We therefore obtained the ratio P'_{app}/P_{app} by plotting $c'_{e,app}\ln\frac{c'-c'_{e,app}}{c'_1-c'_{e,app}}$ versus

898 $c_{\mathrm{e,app}} \ln \frac{c-c_{\mathrm{e,app}}}{c_1-c_{\mathrm{e,app}}}$ (Fig. 9) and calculated $\delta D_{soil,app}$ from Eq. (4). This yielded
899 smaller scatter for $\delta D_{soil,app}$. After retrieving k_{true}, P_{true} and $\alpha_{soil,true}$ as described
900 above, we used the flask sampling model again to derived correction factors by
901 comparing $\delta D_{soil,true}$ used as model input with $\delta D_{soil,app}$ obtained from
902 $c'_{\mathrm{e,app}} \ln \frac{c'-c'_{\mathrm{e,app}}}{c'_1-c'_{\mathrm{e,app}}}$ versus $c_{\mathrm{e,app}} \ln \frac{c-c_{\mathrm{e,app}}}{c_1-c_{\mathrm{e,app}}}$ of the model output, and retrieve
903 $\delta D_{soil,true}$ from $\delta D_{soil,app}$ for each experiment. Fig. 10d shows
904 $(\delta D_{soil,true}+1)/(\delta D_{soil,app}+1)$ as a function of $(\delta D_{soil,app}+1)$ for a $\alpha_{soil,true}$ range of 0.90
905 to 1.00 with the sampling setup described above (V'=22.8 L, f=2 L min^{-1} and
906 Δt=10 min) for k_{true}=0.25 min^{-1} and P_{true}=50 ppb min^{-1}. The ratio
907 $(\delta D_{soil,true}+1)/(\delta D_{soil,app}+1)$ changes from 0.99 to 1.05 for a wide $(\delta D_{soil,app}+1)$
908 range of 0.25 to 0.65. It can be seen that the $(\delta D_{soil,true}+1)/(\delta D_{soil,app}+1)$ ratio
909 depends slightly on $\alpha_{soil,true}$ at a fixed $(\delta D_{soil,app}+1)$, with a maximum difference
910 of about 1% for a $\alpha_{soil,true}$ range of 0.90 to 1.00. The ratio
911 $(\delta D_{soil,true}+1)/(\delta D_{soil,app}+1)$ for each net-emission experiment is shown in Table 3,
912 ranging from 1.007 to 1.048. The largest difference between $\delta D_{soil,true}$ and
913 $\delta D_{soil,app}$ is 21‰ for CBW-8. The mean δD_{true} and δD_{app} for these net emission
914 experiments are -530‰ and -538‰, respectively.
915
916 In conclusion, the effect of the flask sampling process is relatively small for α_{soil}
917 and δD_{soil}, but considerable for the uptake rate constants k and k' and emission
918 rates P and P'. The flask sampling model allows to derive corresponding

corrections that have been applied to correct for the bias introduced by the flask sampling system.

Acknowledgements

We are grateful to C. Van der Veen, M. Bolder and H. Snellen for their help on maintaining the GC-IRMS system and set-up of the sampling. We are also grateful to Jan Kaiser for giving valuable comments on the flask sampling model. This work was supported by the Dutch National Science foundation NWO as part of the NWO-ACTS Sustainable Hydrogen (H_2) project 2007/00566/ACTS, grant numbers 053.61.026 and 053.61.126.

References

Batenburg, A. M., Walter, S., Pieterse, G., Levin, I., Schmidt, M., Jordan, A., Hammer, S., Yver, C., and Röckmann, T.: Temporal and spatial variability of the stable isotopic composition of atmospheric molecular hydrogen: observations at six EUROHYDROS stations, Atmos. Chem. Phys., 11, 6985–6999, doi:10.5194/acp-11-6985-2011, 2011.

Beljaars, A. C. M. and Bosveld, F. C.: Cabauw data for the validation of land surface parameterization schemes, J. Climate, 10, 1172-1193, doi: 10.1175/1520-0442(1997)010<1172:CDFTVO>2.0.CO;2, 1997.

Belnap, J.: Factors influencing nitrogen fixation and nitrogen release in biological soil crusts, Springer-Verlag, Berlin Heidelberg, 241–261, 2001.

Bottinga, Y.: Calculated fractionation factors for carbon and hydrogen isotope exchange in the system calcite-carbon dioxide-graphite-methane-hydrogen-water vapour, Geochim. Cosmochim. Ac., 33, 49–64, doi:10.1016/0016-7037(69)90092-1, 1969.

Conrad, R.: Compensation concentration as critical variable for regulating the flux of trace gases between soil and atmosphere, Biogeochemistry, 27, 155–170, doi:10.1007/BF00000582, 1994.

964

965 Conrad, R. and Seiler W.: Field measurements of hydrogen evolution by nitrogen-
966 fixing legumes, Soil Biol. Biochem., 11, 689-690, doi: 10.1016/0038-0717(79)90041-
967 5, 1979.

968

969 Conrad, R. and Seiler, W.: Contribution of hydrogen production by biological
970 nitrogen fixation to the global hydrogen budget, J. Geophys. Res., 85, 5493-5498, doi:
971 10.1029/JC085iC10p05493, 1980.

972

973 Conrad, R. and Seiler, W.: Decomposition Of atmospheric hydrogen by soil
974 microorganisms and soil enzymes, Soil Biol. Biochem., 13, 43–49, doi: 10.1016/0038-
975 0717(81)90101-2, 1981.

976

977 Conrad, R. and Seiler, W.: Influence of temperature, moisture, and organic carbon on
978 the flux of H_2 and CO between soil and atmosphere: field studies in subtropical
979 regions, J. Geophys. Res., 90, 5699–5709, doi: 10.1029/JD090iD03p05699, 1985.

980

981 Conrad, R., Weber, M., and Seiler, W.: Kinetics and electron transport of soil
982 hydrogenases catalyzing the oxidation of atmospheric hydrogen, Soil Biol. and
983 Biochem., 15, 167-173, doi: 10.1016/0038-0717(83)90098-6, 1983.

984

985 Constant, P., Poissant, L., and Villemur, R.: Isolation of Streptomyces sp. PCB7, the
986 first microorganism demonstrating high-affinity uptake of tropospheric H_2, ISME J., 2,
987 1066-1076, doi: 10.1038/ismej.2008.59, 2008a.
988
989 Constant, P., Poissant, L., and Villemur, R.: Annual hydrogen, carbon monoxide and
990 carbon dioxide concentrations and surface to air exchanges in a rural area (Québec,
991 Canada), Atmos. Environ., 42, 5090-5100, doi: 10.1016/j.atmosenv.2008.02.021,
992 2008b.
993
994 Constant, P., Chowdhury, S. P., Pratscher, J., and Conrad, R.: Streptomycetes
995 contributing to atmospheric molecular hydrogen soil uptake are widespread and
996 encode a putative high-affinity [NiFe]-hydrogenase, Environ. Microbiol., 12, 821-829,
997 doi:10.1111/j.1462-2920.2009.02130.x, 2010.
998
999 Constant, P., Chowdhury, S. P., Hesse, L., and Conrad, R.: Co-localization of
1000 atmospheric H_2 oxidation activity and high affinity H_2-oxidizing bacteria in non-
1001 axenic soil and sterile soil amended with Streptomyces sp. PCB7. Soil Biol.
1002 Biochem., 43, 1888-1893, doi: 10.1016/j.soilbio.2011.05.009, 2011.
1003
1004 De Wit, J. C., Van der Straten, C. M., and Mook, W. G.: Determination of the
1005 absolute isotopic ratio of V-SMOW and SLAP, Geostandards Newsletter, 4, 33–36,
1006 doi:10.1111/j.1751- 908X.1980.tb00270.x, 1980.
1007

1008 Ehhalt, D. H. and Rohrer, F.: The tropospheric cycle of H_2: a critical review, Tellus B,
1009 61(3), 500–535, doi:10.1111/j.1600-0889.2009.00416.x, 2009.
1010
1011 Ehhalt, D. H. and Rohrer, F.: The dependence of soil H_2 uptake on temperature and
1012 moisture: a reanalysis of laboratory data, Tellus B, 63(5), 1040-1051,
1013 doi: 10.1111/j.1600-0889.2011.00581.x, 2011.
1014
1015 Ehhalt, D. H. and Rohrer, F.: Deposition velocity of H_2: a new algorithm for its
1016 dependence on soil moisture and temperature, Tellus B, 65, 19904
1017 doi:10.3402/tellusb.v65i0.19904, 2013a.
1018
1019 Ehhalt, D. H. and Rohrer, F.: Dry deposition of molecular hydrogen in the presence of
1020 H_2 production, Tellus B, 65, 20620, doi:10.3402/tellusb.v65i0.20620, 2013b.
1021
1022 Evans, H. J., Harker, A. R., Papen, H., Russell, S. A., Hanus, F. J., and Zuber, M.:
1023 Physiology, biochemistry, and genetics of the uptake hydrogenase in rhizobia, Annu.
1024 Rev. Microbiol., 41(1), 335-361, 1987.
1025
1026 Gerst, S. and Quay, P.: The deuterium content of atmospheric molecular hydrogen:
1027 Method and initial measurements, J. Geophys. Res., 105, 26433–26445,
1028 doi:10.1029/2000JD900387, 2000.
1029

1030 Förstel, H.: HT to HTO conversion in the soil and subsequent tritium pathway: field
1031 release data and laboratory experiments, Fusion Tech., **14**, 1241–1246, 1988.
1032
1033 Förstel, H. and Führ, F.: Trockene Deposition von Tritium in den Boden, Annual
1034 Report, Forschungszentrum Jülich, Jülich, 45–51, 1992.
1035
1036 Gerst, S. and Quay, P.: Deuterium component of the global molecular hydrogen cycle,
1037 J. Geophys. Res., 106, 5021–5031, doi:10.1029/2000JD900593, 2001.
1038
1039 Gonfiantini, R., Stichler, W., and Rozanski, K.: Standards and intercomparison
1040 materials distributed by the International Atomic Energy Agency for stable isotope
1041 measurements, in: Reference and intercomparison materials for stable isotopes of light
1042 elements: Proceedings of a consultants meeting held in Vienna, 1-3 December 1993,
1043 IAEA-TECDOC-825, International Atomic Energy Agency, Vienna, 1993.
1044
1045 Guo, R. and Conrad, R.: Extraction and characterization of soil hydrogenases
1046 oxidizing atmospheric hydrogen, Soil Biol. Biochem., 40(5), 1149–1154,
1047 doi:10.1016/j.soilbio.2007.12.007, 2008.
1048
1049 Häring, V., Klüber, H. D., and Conrad, R.: Localization of atmospheric H_2-oxidizing
1050 soil hydrogenases in different particle fractions of soil, Biol. Fert. Soils, 18(2), 109-
1051 114, doi:10.1007/BF00336455, 1994.
1052

1053 Haumann, F. A., Batenburg, A. M., Pieterse, G., Gerbig, C., Krol, M. C., and
1054 Röckmann, T.: Emission ratio and isotopic signatures of molecular hydrogen
1055 emissions from tropical biomass burning, Atmos. Chem. Phys., 13, 9401–9413,
1056 doi:10.5194/acp-13-9401-2013, 2013.
1057
1058 Heij, G. H. and Erisman, J. W.: Acid Atmospheric Deposition and Its Effects on
1059 Terrestrial Ecosystems in The Netherlands, Studies in Environmental Sciences 69,
1060 ISBN 0-444-82037-X, Elsevier, Amsterdam, 1997.
1061
1062 Hoffmann, G., Werner, M., and Heimann, M.: The water isotope module of the
1063 ECHAM atmospheric general circulation model – A study on time scales from days to
1064 several years, J. Geophys. Res., 103, 16871–16896, doi:10.1029/98JD00423, 1998.
1065
1066 Jordan, A. and Steinberg, B.: Calibration of atmospheric hydrogen measurements,
1067 Atmos. Meas. Tech., 4, 509–521, doi:10.5194/amt-4-509-2011, 2011.
1068
1069 Kawagucci, S., Toki, T., Ishibashi, J., Takai, K., Ito, M., Oomori, T., and Gamo, T.,
1070 Isotopic variation of molecular hydrogen in 20°–375°C hydrothermal fluids as
1071 detected by a new analytical method, J. Geophys. Res., 115, G03021,
1072 doi:10.1029/2009JG001203, 2010.
1073
1074 Khdhiri, M., Hesse, L., Popa, M. E., Quiza, L., Lalonde, I., Meredith, L. K.,
1075 Röckmann, T., and Constant, P.: Soil carbon content and relative abundance of high

affinity H_2-oxidizing bacteria predict atmospheric H_2 soil uptake activity better than soil microbial community composition, Soil Biol. Biochem., 85, 1-9, doi:10.1016/j.soilbio.2015.02.030, 2015.

Kreuzer-Martin, H. W., Lott, M. J., Ehleringer, J. R., and Hegg, E. L.: Metabolic processes account for the majority of the intracellular water in log-phase Escherichia coli cells as revealed by hydrogen isotopes, Biochemistry, 45(45), 13622-13630, doi:10.1021/bi0609164, 2006.

Luo, Y., Sternberg, L., Suda, S., Kmazawa, S., and Mitsui, A.: Extremely low D/H ratios of photoproduced hydrogen by cyanobacteria, Plant Cell Physiol., 32(6), 897–900, 1991.

Meredith, L.K.: Field measurement of the fate of atmospheric H_2 in a Forest environment: from canopy to soil, Ph.D. thesis, Department of Earth, Atmospheric and Planetary Sciences, Massachusetts Institute of Technology, United States, 250 pp, 2012.

Novelli, P. C., Lang, P. M., Masarie, K. A., Hurst, D. F., Myers, R., and Elkins, J. W.: Molecular hydrogen in the troposphere: Global distribution and budget, J. Geophys. Res., 104, 30427– 30444, doi:10.1029/1999JD900788, 1999.

1098 Pieterse, G., Krol, M. C., Batenburg, A. M., Steele, L. P., Krummel, P. B.,
1099 Langenfelds, R. L., and Röckmann, T.: Global modelling of H_2 mixing ratios and
1100 isotopic compositions with the TM5 model, Atmos. Chem. Phys., 11, 7001–7026,
1101 doi:10.5194/acp- 11-7001-2011, 2011.
1102
1103 Pieterse, G., Krol, M. C., Batenburg, A. M., Brenninkmeijer, C. A. M., Popa, M. E.,
1104 O'Doherty, S., Grant, A., Steele, L. P., Krummel, P. B., Langenfelds, R. L., Wang, H.
1105 J., Vermeulen, A. T., Schmidt, M., Yver, C., Jordan, A., Engel, A., Fisheraffilmark, R.
1106 E., Lowry, D., Nisbet, E. G., Reimann, S., Vollmer, M. K., Steinbacher, M., Hammer,
1107 S., Forster, G., Sturges, W. T., and Röckmann, T.: Reassessing the variability in
1108 atmospheric H_2 using the two-way nested TM5 model, J. Geophys. Res.-Atmos., 118,
1109 3764–3780, doi:10.1002/jgrd.50204, 2013.
1110
1111 Popa, M. E., Vermeulen, A. T., van den Bulk, W. C. M., Jongejan, P. A. C.,
1112 Batenburg, A. M., Zahorowski, W., and Röckmann, T.: H_2 vertical profiles in the
1113 continental boundary layer: measurements at the Cabauw tall tower in the Netherlands,
1114 Atmos. Chem. Phys., 11, 6425–6443, doi:10.5194/acp-11-6425-2011, 2011.
1115
1116 Price, H., Jaeglé, L., Rice, A., Quay, P., Novelli, P. C., and Gammon, R.: Global
1117 budget of molecular hydrogen and its deuterium content: Constraints from ground
1118 station, cruise, and aircraft observations, J. Geophys. Res .-Atmos., 112, D22108,
1119 doi:10.1029/2006JD008152, 2007.
1120

1121 Rahn, T., Eiler, J. M., Kitchen, N., Fessenden, J. E., and Randerson, J. T.:
1122 Concentration and δD of molecular hydrogen in boreal forests: Ecosystem-scale
1123 systematics of atmospheric H_2, Geophys. Res. Lett., 29(18), 35-1-35-4,
1124 doi:10.1029/2002GL015118, 2002a.
1125
1126 Rahn, T., Kitchen, N., and Eiler, J.: D/H ratios of atmospheric H_2 in urban air: results
1127 using new methods for analysis of nano-molar H_2 samples, Geochim. Cosmochim.
1128 Ac., 66(14), 2475– 2481, doi:10.1016/S0016-7037(02)00858-X, 2002b.
1129
1130 Rahn, T., Eiler, J. M., Boering, K. A., Wennberg, P. O., McCarthy, M. C., Tyler, S.,
1131 Schauffler, S., Donnelly, S., and Atlas, E.: Extreme deuterium enrichment in
1132 stratospheric hydrogen and the global atmospheric budget of H_2, Nature, 424, 918–
1133 921, doi:10.1038/nature01917, 2003.
1134
1135 Rahn, T., Randerson, J. T., and Eiler, J.: Variability of Deuterium Fractionation
1136 Associated With Soil Uptake of Atmospheric Molecular Hydrogen, Eos Trans. AGU,
1137 86(52), Fall Meet. Suppl., Abstract B11A-1031, 2005
1138
1139 Rhee, T. S., Mak, J., Röckmann, T., and Brenninkmeijer, C. A. M.: Continuous-flow
1140 isotope analysis of the deuterium/hydrogen ratio in atmospheric hydrogen, Rapid
1141 Commun. Mass Spectrom., 18(3), 299–306, doi:10.1002/rcm.1309, 2004.
1142

1143 Rice, A., Quay, P., Stutsman, J., Gammon, R., Price, H., and Jaeglé, L.: Meridional
1144 distribution of molecular hydrogen and its deu- terium content in the atmosphere, J.
1145 Geophys. Res., 115(D12), 1–12, doi:10.1029/2009JD012529, 2010.
1146
1147 Rice, A., Dayalu, A., Quay, P., and Gammon, R.: Isotopic fractionation during soil
1148 uptake of atmospheric hydrogen, Biogeosciences, 8, 763–769, doi:10.5194/bg-8-763-
1149 2011, 2011.
1150
1151 Röckmann, T., Rhee, T. S., and Engel, A.: Heavy hydrogen in the stratosphere, Atmos.
1152 Chem. Phys., 3, 2015–2023, doi:10.5194/acpd-3-3745-2003, 2003a.
1153
1154 Röckmann, T., Kaiser, J., Brenninkmeijer, C. A. M., and Brand, W. A.: Gas
1155 chromatography/isotope-ratio mass spectrometry method for high-precision position-
1156 dependent ^{15}N and ^{18}O measurements of atmospheric nitrous oxide, Rap. Commun.
1157 Mass Spectrom., 17, 1897-1908, 2003b.
1158
1159 Röckmann, T., Álvarez, C. X. G., Walter, S., Veen, C. van der, Wollny, A. G., Gunthe,
1160 S. S., Helas, G., Pöschl, U., Keppler, F., Greule, M., and Brand, W. A.: Isotopic
1161 composition of H_2 from wood burning: Dependency on combustion efficiency,
1162 moisture content, and δD of local precipitation, J. Geophys. Res., 115, D17308,
1163 doi:10.1029/2009JD013188, 2010.
1164

1165 Rothe, M., Jordan, A., and Brand, W. A.: Trace gases, δ13C and δ18O of CO2-in-air
1166 samples: Storage in glass flasks using PCTFE seals and other effects, in: GAW report
1167 161,12th WMO/IAEA meeting of experts on carbon dioxide concentration and related
1168 tracers measurements techniques, edited by: Worthy, D. and Huang, L., Toronto,
1169 Canada, 15–18 September 2003, WMO TD No. 1275, 2004.
1170
1171 Ruijven, B. van, Lamarque, J. F., Vuuren, D. P. van, Kram, T., and Eerens, H.:
1172 Emission scenarios for a global hydrogen economy and the consequences for global
1173 air pollution, Global Environ. Chang., 21(3), 983-994, 2011.
1174
1175 Schmitt, S., Hanselmann, A., Wollschläger, U., Hammer, S., and Levin, I.:
1176 Investigation of parameters controlling the soil sink of atmospheric molecular
1177 hydrogen. Tellus B, 61(2), 416-423, 2009.
1178
1179 Schultz, M. G., Diehl, T., Brasseur, G. P., and Zittel, W.: Air pollution and climate-
1180 forcing impacts of a global hydrogen economy, Science, 302(5645), 624–627,
1181 doi:10.1126/science.1089527, 2003.
1182
1183 Smith-Downey, N. V., Randerson, J. T. and Eiler, J. M.: Temperature and moisture
1184 dependence of soil H_2 uptake measured in the laboratory. Geophys. Res. Lett., 33,
1185 L14813, doi:10.1029/2006GL026749, 2006.
1186

1187 Smith-Downey, N. V., Randerson, J. T., and Eiler, J. M.: Molecular hydrogen uptake
1188 by soils in forest, desert, and marsh ecosystems in California, J. Geophys. Res.-
1189 Biogeosci., 113, G03037, doi:10.1029/2008JG000701, 2008.
1190
1191 Tromp, T. K., Shia, R. L., Allen, M., Eiler, J. M., and Yung, Y. L.: Potential
1192 environmental impact of a hydrogen economy on the stratosphere, Science, 300,
1193 1740–1742, doi:10.1126/science.1085169, 2003.
1194
1195 Vogel, B., Feck, T., Grooβ, J. U., and Riese, M.: Impact of a possible future global
1196 hydrogen economy on Arctic stratospheric ozone loss, Energy Environ. Sci., 5, 6445-
1197 6452, doi:10.1039/c2ee03181g, 2012.
1198
1199 Vollmer, M. K., Walter, S., Mohn, J., Steinbacher, M., Bond, S. W., Röckmann, T.,
1200 and Reimann, S.: Molecular hydrogen (H_2) combustion emissions and their isotope
1201 (D/H) signatures from domestic heaters, diesel vehicle engines, waste incinerator
1202 plants, and biomass burning, Atmos. Chem. Phys., 12, 6275–6289, doi:10.5194/ acp-
1203 12-6275-2012, 2012.
1204
1205 Walter, S., Laukenmann, S., Stams, A. J. M., Vollmer, M. K., Gleixner, G., and
1206 Röckmann, T.: The stable isotopic signature of biologically produced molecular
1207 hydrogen (H_2). Biogeosciences, 9(10), 4115-4123, 2012.
1208

Warwick, N. J., Bekki, S., Nisbet, E. G., and Pyle, J. A.: Impact of a hydrogen economy on the stratosphere and troposphere studied in a 2-D model, Geophys. Res. Lett., 31(5), 2–5, doi:10.1029/2003GL019224, 2004.

Xiao, X., Prinn, R. G., Simmonds, P. G., Steele, L. P., Novelli, P. C., Huang, J., Langenfelds, R. L., O'Doherty, S., Krummel, P. B., Fraser, P. J., Porter, L. W., Weiss, R. F., Salameh, P., and Wange, R. H. J.: Optimal estimation of the soil uptake rate of molecular hydrogen from the Advanced Global Atmospheric Gases Experiment and other measurements, J. Geophys. Res., 112, D07303, doi:10.1029/2006JD007241, 2007.

Yang, H., Gandhi, H., Shi, L., Kreuzer, H. W., Ostrom, N. E., and Hegg, E. L.: Using gas chromatography/isotope ratio mass spectrometry to determine the fractionation factor for H_2 production by hydrogenases. Rapid Commun. Mass Spectrom., 26(1), 61-68, doi: 10.1002/rcm.5298, 2012.

Tables

Table 1. The deposition velocity (v_d), fractionation factor (α_{soil}) as well as its error estimate, and soil cover information for each Speuld experiment (a) and Cabauw net-uptake experiment (b). The STDEV represents standard deviation and SE represents standard error. The errors of α_{soil} represent the 95% confidence interval (CI) for $\alpha_{soil,app}$ obtained from $\ln\frac{c'-c'_{e,app}}{c'_1-c'_{e,app}}$ versus $\ln\frac{c-c_{e,app}}{c_1-c_{e,app}}$.

(a)	F_n (nmol m^{-2} s^{-1})	v_d (cm s^{-1})	α_{soil}	Error α_{soil}	soil cover
SPU-1	-30.1	0.20	0.924	0.032	D. fir, moss
SPU-2	-35.3	0.22	0.948	0.028	D. fir, needles
SPU-3	-37.7	0.20	0.945	0.008	D. fir, moss
SPU-4	-26.1	0.16	0.913	0.004	D. fir, moss
SPU-5	-24.9	0.16	0.918	0.006	D. fir, moss
SPU-6	-13.2	0.12	0.951	0.031	D. fir, moss
SPU-7	-19.6	0.12	0.939	0.005	beech, leaves
SPU-8	-28.4	0.16	0.955	0.008	*Same subsite as SPU-7, leaves removed*
SPU-9	-20.4	0.12	0.925	0.002	beech, leaves
SPU-10	-22.3	0.13	0.949	0.060	spruce, moss
SPU-11	-19.4	0.13	0.936	0.068	spruce, needles
SPU-12	-40.5	0.28	0.947	0.004	*Same subsite as SPU-11, needles removed*
MEAN	-26.5	0.17	0.937	/	/

STDEV	8.2	0.05	0.014	/	/
SE	2.4	0.01	0.004	/	/

1236

1237

(b)	F_n (nmol m^{-2} s^{-1})	v_d (cm s^{-1})	α_{soil}	Error α_{soil}	soil cover
CBW-5	-6.6	0.04	0.943	0.004	few clover, grass
CBW-7	-3.1	0.03	1.019	0.005	few clover, grass
CBW-16	-22.9	0.18	0.993	0.001	bare soil, few grass
CBW-18	-39.3	0.24	0.950	0.054	grass
CBW-19	-7.4	0.14	0.935	0.105	grass
CBW-20	-14.9	0.20	0.940	0.260	bare soil
CBW-25	-8.0	0.12	0.911	0.014	clover, grass
CBW-26	-6.1	0.09	0.916	0.038	grass
MEAN	-13.6	0.13	0.951	/	/
STDEV	12.2	0.08	0.037	/	/
SE	4.3	0.03	0.013	/	/

1238 Table 2. Net flux, deposition velocity and δD_{soil} (including error) obtained from the mass
1239 balance model for the net H_2 emission experiments.

Net emission	F_n (nmol m^{-2} s^{-1})	v_d (cm s^{-1})	δD_{soil} (‰)	Error δD_{soil} (‰)
CBW-8	24.5	0.05	-535	53
CBW-10	16.1	0.03	-460	17
CBW-14	13.7	0.02	-629	21
CBW-17	20.3	0.03	-542	1
CBW-21	42.0	0.04	-574	3
CBW-28	150.2	0.14	-488	83
CBW-30	41.0	0.05	-580	7
CBW-31	92.0	0.09	-509	7
CBW-33	46.2	0.10	-451	52
MEAN	49.5	0.06	-530	/
STDEV	44.7	0.04	59	/
SE	14.9	0.01	20	/

Table 3. Sampling information and the correction coefficients (k_{true}/k_{app}, P_{true}/P_{app}, $\alpha_{soil,true}/\alpha_{soil,app}$ and $(\delta D_{soil,true}+1)/(\delta D_{soil,app}+1)$ used for each experiments. Size S refers to small chamber and size L refers to large chamber.

Exp.	Pressure (kPa)	Flow rate (L min^{-1})	Size	Δt (min)	k_{app} (min^{-1})	P_{app} (ppb min^{-1})	k_{true}/k_{app}	P_{true}/P_{app}	$\alpha_{soil,true}/\alpha_{soil,app}$	$(\delta D_{soil,true}+1)/(\delta D_{soil,app}+1)$
SPU-1	200	2	S	10	0.199	4.12	1.494	1.601	0.984	/
SPU-2	200	2.2	S	5	0.206	0.67	1.589	7.472	0.998	/
SPU-3	200	3.1	S	5	0.204	3.58	1.496	2.475	0.999	/
SPU-4	200	2.8	S	5	0.160	7.51	1.526	2.136	1.004	/
SPU-5	200	2.6	S	5	0.156	4.16	1.546	2.759	1.004	/
SPU-6	160	3.2	L	5	0.232	7.61	1.184	1.446	0.999	/
SPU-7	160	3.2	S	5	0.128	5.40	1.418	2.264	1.006	/
SPU-8	160	2.5	S	5	0.172	4.23	1.438	2.381	1.001	/
SPU-9	160	2.8	S	5	0.128	4.56	1.440	2.513	1.007	/
SPU-10	180	2.7	S	5	0.128	/	1.502	/	1.005	/
SPU-11	160	2.2	S	5	0.130	/	1.490	/	1.006	/
SPU-12	180	2.3	S	5	0.272	11.30	1.529	1.720	0.994	/
CBW-5	200	2	L	10	0.086	18.24	1.204	1.248	1.001	/
CBW-7	200	1.9	L	10	0.048	11.57	1.260	1.361	0.999	/
CBW-16	210	2.1	S	10	0.183	45.21	1.498	1.505	0.999	/
CBW-18	200	2	S	10	0.240	38.07	1.532	1.527	0.986	/
CBW-19	200	2	S	10	0.145	56.69	1.457	1.463	0.991	/
CBW-20	200	2	S	10	0.196	65.81	1.491	1.494	0.988	/
CBW-25	200	2	S	10	0.122	44.85	1.449	1.460	0.994	/
CBW-26	200	2	S	10	0.088	31.05	1.452	1.475	1.002	/
CBW-8	200	2	S	10	0.044	82.92	1.542	1.438	/	1.048
CBW-10	200	2.6	L	10	0.069	111.00	1.177	1.152	/	1.010
CBW-14	200	2.5	L	10	0.035	82.53	1.251	1.166	/	1.042
CBW-17	220	2.1	L	10	0.047	117.40	1.268	1.198	/	1.024

CBW-21	220	2	L	10	0.078	232.20	1.209	1.179	/	1.008
CBW-28	175	1.8	S	10	0.146	440.90	1.412	1.402	/	1.018
CBW-30	200	2	L	10	0.090	237.70	1.202	1.180	/	1.008
CBW-31	200	2	S	10	0.098	275.10	1.451	1.422	/	1.007
CBW-33	200	2	S	10	0.107	166.50	1.449	1.430	/	1.007

Figures

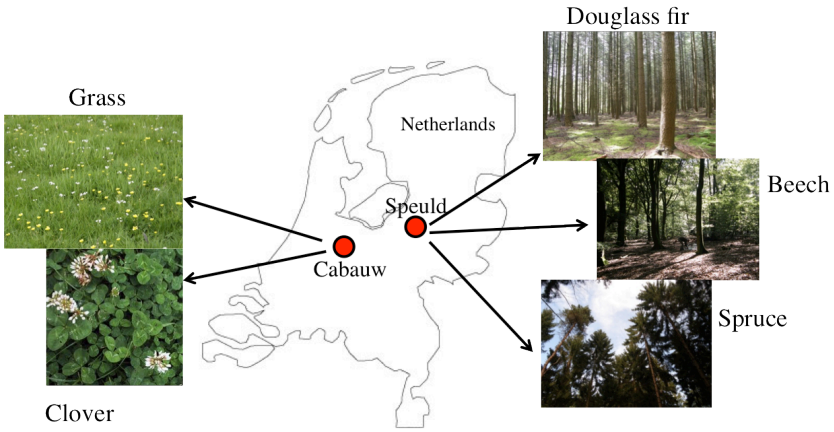

Fig. 1. The location of the two sampling sites (Cabauw and Speuld) in the Netherlands, as well as the plant species there.

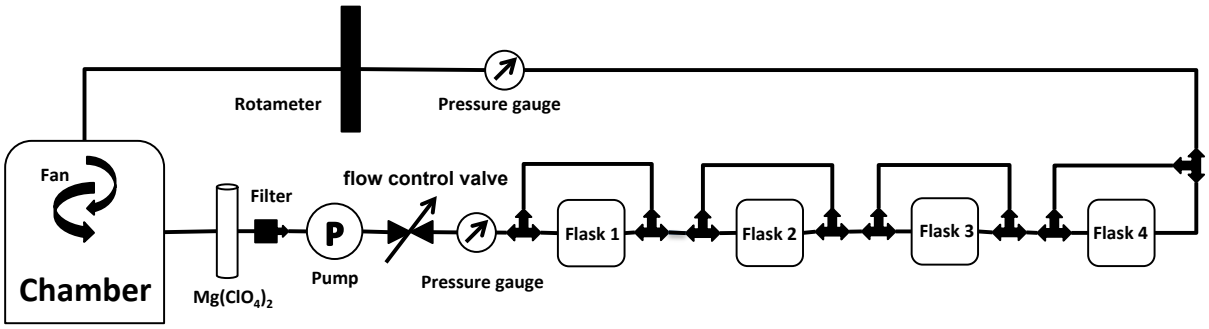

Fig. 2. Scheme of the sampling setup using the closed-cycle air sampler. The volume of the soil chamber was 22.8 L and the volume of each flask was 1 L.

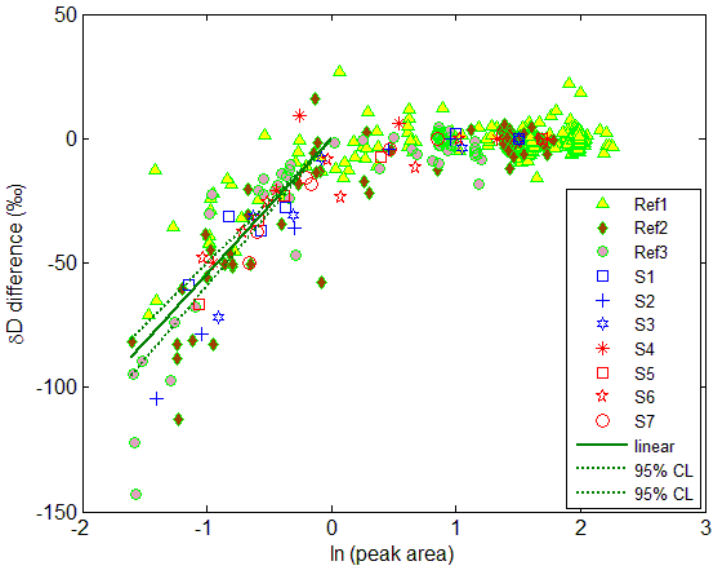

Fig. 3. Difference of δD from the assigned value for different gases including reference gases (Ref1-3) and laboratory flask samples (S1-7). A linear function (y = 54.6x) was fit to the data with peak area between 0.2 and 1.0 V s (green solid line; the dashed lines represent the 95% confidence interval of the fit). This function was used to correct the soil experiment data that were measured at low peak areas.

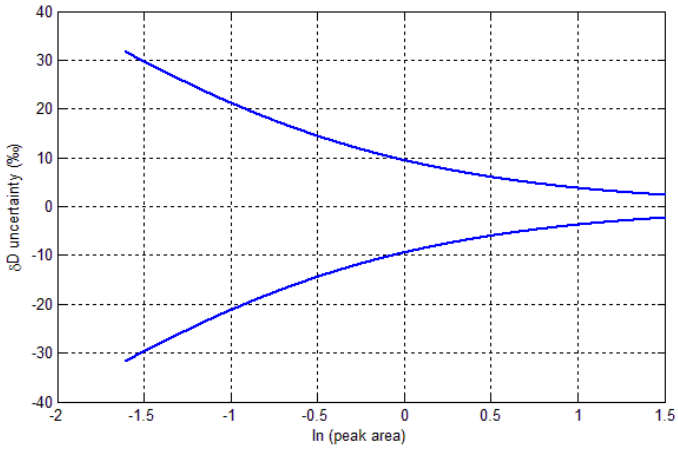

Fig. 4. Calculated total assigned uncertainty of δD (consisting of analytical uncertainty and uncertainty arising from the linearity correction) for air samples with ln(peak area) ranging from -1.6 to 1.5.

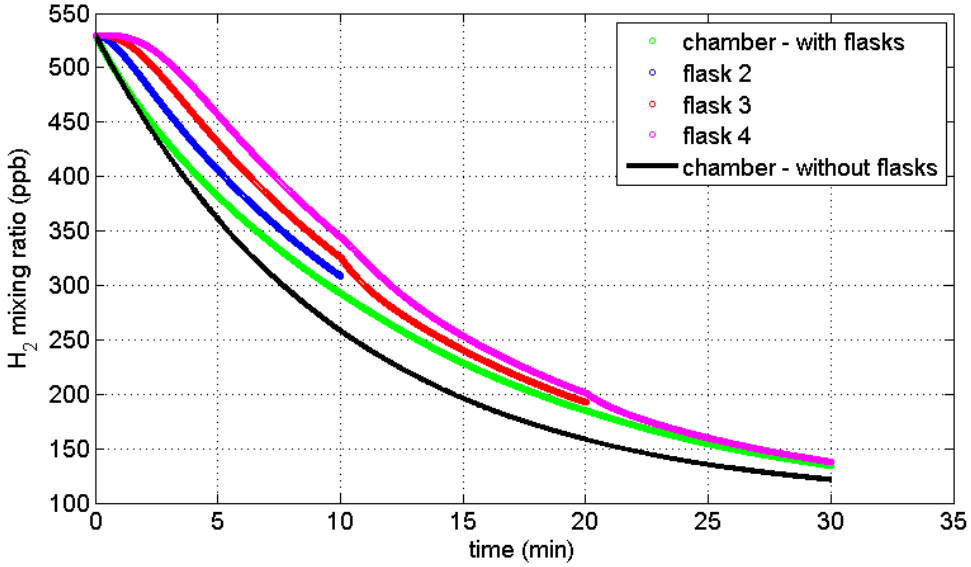

Fig. 5. Results of the flask sampling model with the following parameters: k=0.1 min^{-1}, P=10 ppb min^{-1} and $c_1(t=0)$=530 ppb. The figure shows the evolution of H_2 mole fraction in the chamber (green curve), in flask 2 (blue curve), flask 3 (red curve) and flask 4 (magenta curve) as a function of time, and what would be expected for a chamber without flasks (black curve). Flask 1 was closed before closing the chamber (at time 0 when all volumes contained the same air).

1338

1339

1340

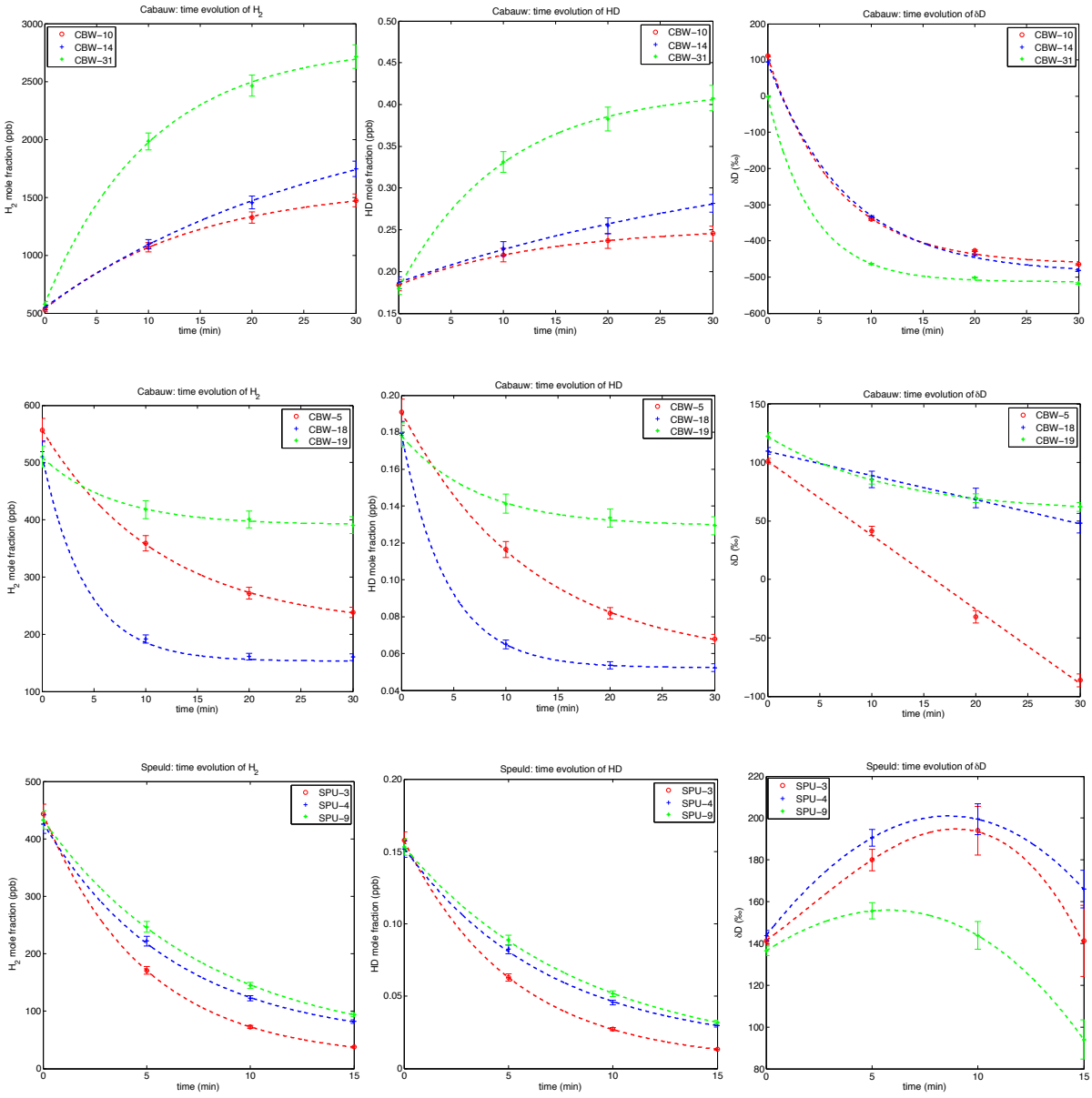

1341 Fig. 6. Time evolution of H_2, HD and δD in Cabauw (upper and middle panels) and in Speuld
1342 (lower panel) for representative experiments. HD is calculated from H_2 and δD. The H_2 data
1343 are fitted with an exponential function of the form: $c = \left(c_1 - c_{\mathrm{e,app}}\right)e^{-k_{app}t} + c_{\mathrm{e,app}}$, where
1344 c_1 and $c_{\mathrm{e,app}}$ are the H_2 mole fractions initially and in equilibrium, and k_{app} is the apparent soil
1345 uptake rate constant for H_2. A similar exponential function is applied to the HD data. Error
1346 estimates for H_2, HD and δD are shown. The connecting lines for δD data are included to
1347 guide the eye.

1348

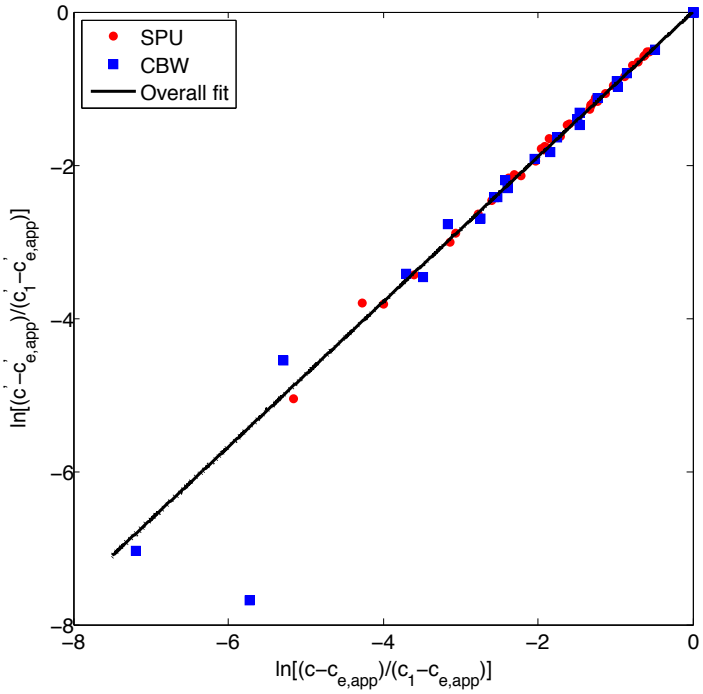

Fig. 7. Plot of $\ln\frac{c'-c'_{e,app}}{c'_1-c'_{e,app}}$ versus $\ln\frac{c-c_{e,app}}{c_1-c_{e,app}}$ for all Speuld and Cabauw net-uptake experiments. The slope of the linear fit to the data returns the fractionation factor $\alpha_{soil,app}$=0.947±0.004 (95% CI). Errors in x and y direction for each data point were considered. One outlier ("CBW-18") was not included in the fitting. The 95% confidence intervals of the fit line are included as dashed lines but largely overlap with the fit line.

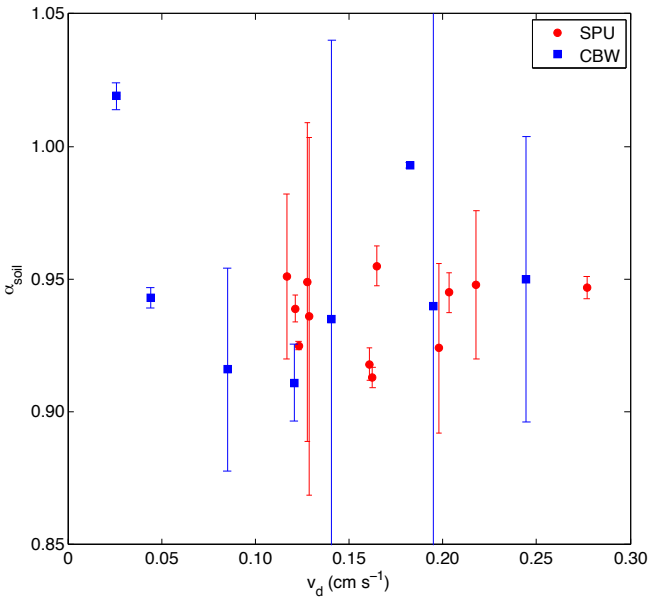

Fig. 8. Correlation between α_{soil} and v_d for all Speuld experiments and Cabauw net-uptake experiments. The errors for α_{soil} were taken from Table 1.

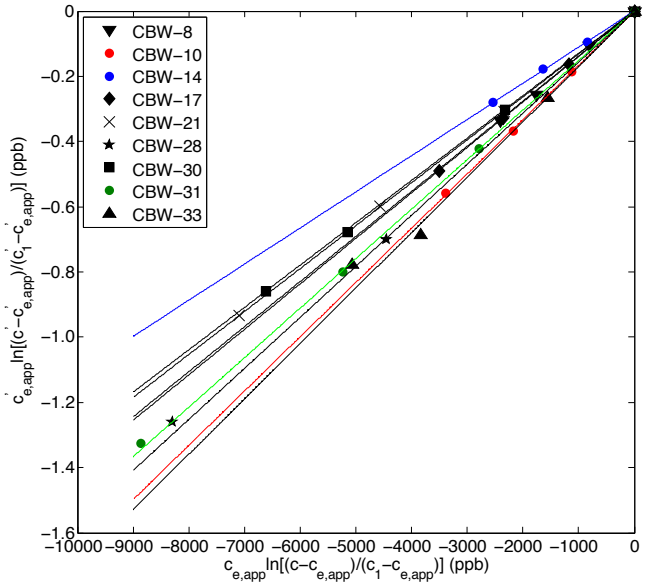

Fig. 9. Plot of $c'_{\mathrm{e,app}} \ln \frac{c'-c'_{\mathrm{e,app}}}{c'_1-c'_{\mathrm{e,app}}}$ versus $c_{\mathrm{e,app}} \ln \frac{c-c_{\mathrm{e,app}}}{c_1-c_{\mathrm{e,app}}}$ for 9 Cabauw net-emission experiments. A linear function was fit to each individual dataset and the slope was used to calculate the $\delta \mathrm{D}_{\mathrm{soil,app}}$ value for each experiment. Errors in x and y direction for each data point were considered.

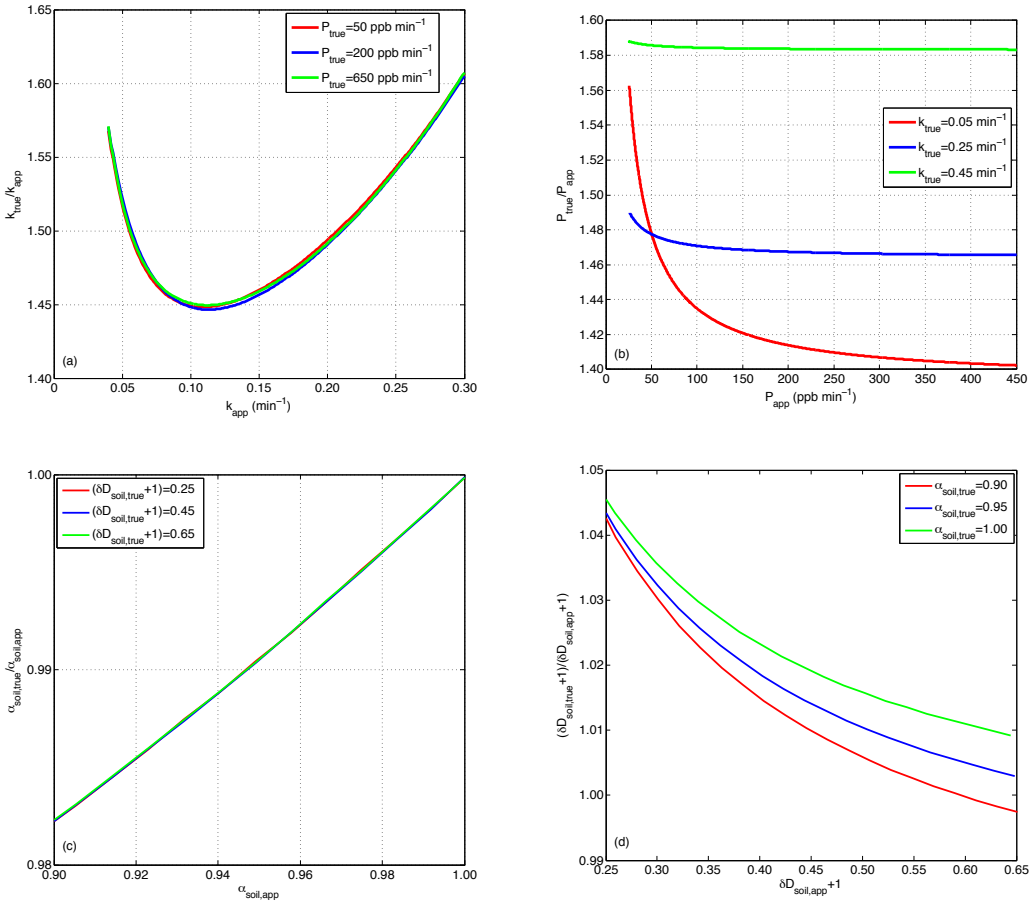

Fig. 10. (a) The relationship between k_{true}/k_{app} and k_{app} for P_{true} of 50, 200 and 650 ppb min^{-1}; (b) between P_{true}/P_{app} and P_{app} for k_{true} of 0.05, 0.25 and 0.45 min^{-1}; (c) between $\alpha_{soil,true}/\alpha_{soil,app}$ and $\alpha_{soil,app}$ for ($\delta D_{soil,true}$+1) of 0.25 to 0.65 for k_{true}=0.25 min^{-1} and P_{true}= 50 ppb min^{-1}; (d) between ($\delta D_{soil,true}$+1) /($\delta D_{soil,app}$+1) and ($\delta D_{soil,app}$+1) for $\alpha_{soil,true}$ of 0.90 to 1.00 for k_{true}=0.25 min^{-1} and P_{true}= 50 ppb min^{-1}. The parameters of the sampling setup are V' =22.8 L, f=2 L min^{-1}, Δt=10 min and the pressures inside the flasks and chamber are 200 kPa and 100 kPa respectively.